SOOT FORMATION IN INDUSTRIAL BURNERS

A THESIS SUBMITTED TO
THE GRADUATE SCHOOL OF NATURAL AND APPLIED SCIENCES
OF
MIDDLE EAST TECHNICAL UNIVERSITY

BY

İLKEM HIRTISLI

IN PARTIAL FULFILLMENT OF THE REQUIREMENTS
FOR
THE DEGREE OF MASTER OF SCIENCE
IN
MECHANICAL ENGINEERING

AUGUST 2019

Approval of the thesis:

SOOT FORMATION IN INDUSTRIAL BURNERS

submitted by **İLKEM HIRTISLI** in partial fulfillment of the requirements for the degree of **Master of Science in Mechanical Engineering Department, Middle East Technical University** by,

Prof. Dr. Halil Kalıpçılar
Dean, Graduate School of **Natural and Applied Sciences** _____

Prof. Dr. M. A. Sahir Arıkan
Head of Department, **Mechanical Engineering** _____

Assist. Prof. Dr. Feyza Kazanç Özerinç
Supervisor, **Mechanical Engineering, METU** _____

Examining Committee Members:

Prof. Dr. Ahmet Yozgatlıgil
Mechanical Engineering, METU _____

Assist. Prof. Dr. Feyza Kazanç Özerinç
Mechanical Engineering, METU _____

Assoc. Prof. Dr. M. Metin Yavuz
Mechanical Engineering, METU _____

Assoc. Prof. Dr. Çağlar Sınayuç
Petroleum and Natural Gas Engineering, METU _____

Assoc. Prof. Dr. Murat Kadri Aktaş
Mechanical Engineering, TOBB _____

Date: 29.08.2019

I hereby declare that all information in this document has been obtained and presented in accordance with academic rules and ethical conduct. I also declare that, as required by these rules and conduct, I have fully cited and referenced all material and results that are not original to this work.

Name, Surname: İlkem Hırtıslı

Signature:

ABSTRACT

SOOT FORMATION IN INDUSTRIAL BURNERS

Hırtıslı, İlkem
Master of Science, Mechanical Engineering
Supervisor: Assist. Prof. Dr. Feyza Kazanç Özerinç

August 2019, 82 pages

This thesis examines the problem of soot (also known as coke) formation in industrial burners by thermal methods and morphological characterization. The fuel gas soot (FG) was collected during maintenance stop(s) of a burner in which refinery fuel gas (RFG) is burned. The obtained sample is crushed in a mortar and sieved to 75-106 μm, to minimize particle diameter effects. Thermogravimetric analysis (TGA) is used to determine the combustion characteristic temperatures of the sample. In the TGA experiments which are carried out at non-isothermal conditions, four main characteristic temperatures were determined: the temperature at which devolatilization starts (T_v) ~630-640 °C, the temperature at which the sample ignites (T_i) ~700-720 °C, the highest reaction rate temperature (T_p) ~815-830 °C and the burnout temperature (T_e) ~915-920 °C. Non-isothermal TGA trials allowed to find the target temperature (T_t) for the isothermal trials. For the evaluation of the sample content, a Fourier Transform Infrared Spectroscopy (FTIR) instrument connected to the TGA is used to examine the CO_2, CO, H_2O and SO_x emissions. While CO_2 and CO molecules exist from ignition until burnout, no signs of H_2O and SO_x molecules are observed. Considering the RFG composition, this is an unexpected situation and further evaluation was needed. The X-ray Diffraction (XRD) method is applied and graphite with 2H-crystal structure is observed. To provide further insight, Energy Dispersive

X-Ray (EDX) analysis is applied and it is determined that the substance content is carbon. Because Scanning Electron Microscope (SEM) images were composed of non-crystalline carbon structures, which is in contradiction with the XRD results, RAMAN method is applied, and the sample content is found to be amorphous carbon. Therefore, the sample content is heterogeneous, but the dominant form is amorphous carbon. The morphology of the soot is also examined with SEM and High-Resolution Transmission Electron Microscopy (HRTEM) methods. SEM images show that the particles of various geometry and sizes exist in agglomerated forms. Observation of the surfaces of these structures revealed chain-like carbon structures. For further evaluation of morphology, HRTEM method is used and the mentioned carbon chains are examined closely. In this method, it is observed that the carbonaceous structure did not contain any graphene plane, but some crystalline nodes in amorphous matrix and deviations of interatomic distances in the order of mesoscopic scale ($\simeq$1 nm) exist.

Keywords: Soot, Burner, TGA, Coke, RFG

ÖZ

ENDÜSTRİYEL BRÜLÖRLERDE KURUM OLUŞUMU

Hırtıslı, İlkem
Yüksek Lisans, Makina Mühendisliği
Tez Danışmanı: Dr. Öğr. Üyesi Feyza Kazanç Özerinç

Ağustos 2019, 82 sayfa

Bu tez, endüstriyel brülörlerde görülen kurum oluşumu (koklaşma) sorununu ısıl yöntemler ve morfolojik karakterizasyon ile incelemektedir. İncelenen numune (FG), rafineri yakıt gazı (RFG) yakılan ve tıkanıklık nedeniyle bakıma alınmış olunan bir brülörden elde edilmiştir. Elde edilen numune, havanda ezilmiş ve parçacık çapı etkisini minimuma indirgemek için eleklerden geçirilerek çapı 75-106 μm aralığına getirilip toplanmıştır. Yapılan termogravimetrik analizler (TGA), numunenin yanma karakteristik sıcaklıklarını tespit etmekte kullanılmıştır. Değişken sıcaklıklarda yapılan TGA deneylerinde dört ana karakteristik sıcaklık tespit edilmiştir: Uçucuların örneği terk etmeye başladığı sıcaklık (T_v) ~630-640 °C, numunenin tutuşmaya başladığı sıcaklık (T_i) ~700-720 °C, yanma tepkimesinin en hızlı olduğu andaki sıcaklık (T_p) ~815-830 °C ve yanmanın tamamlandığı sıcaklık ise (T_e) ~915-920 °C olmuştur. Sabit sıcaklıkta yapılan TGA deneyinde, değişken sıcaklıkta bulunmuş olunan T_i sıcaklığı incelenmiştir. Numune içeriğinin değerlendirilmesi adına, CO_2, CO, H_2O ve SO_x salınımlarını incelemek için TGA'ya bağlanmış bir Fourier Dönüşümlü Kızılötesi Spektrometrisi (FTIR) cihazı kullanılmıştır. FTIR sonuçlarında CO_2, CO gözlenirken H_2O ve SO_x moleküllerine rastlanmamıştır. Bu durum RFG kompozisyonundaki değerlerle çeliştiği için X-Işını Difraktometresi (XRD) yöntemine başvurulmuş, sonucunda 2H-kristal yapısına sahip grafit tespit edilmiştir.

Bu durumu doğrulamak için Enerji Saçılımlı X-Işını (EDX) analizine başvurulmuş ve madde içeriğinin karbon olduğu ancak Taramalı Elektron Mikroskobu (SEM) görüntülerinin kristal yapıda olmayan karbonlu yapılardan oluştuğunun tespit edilmesi üzerine RAMAN analiz yöntemine başvurulmuş ve numune içeriğinde amorf yapıda karbon olduğu tespit edilmiştir. Bu nedenle numune içeriğinin heterojen yapıda olduğu ancak baskın formun amorf karbon olduğuna kanaat getirilmiştir. Oluşan kurumun morfolojisi de incelenmiş olup SEM ve Yüksek Çözünürlüklü Transmisyon Elektron Mikroskobu (HRTEM) yöntemlerine başvurulmuştur. SEM görüntülerinde çeşitli geometri ve büyüklükte, topaklanmış yapıda parçacıkların olduğu görülmüştür. Bu yapıların yüzeylerine bakıldığında zincir şeklinde karbonlu yapılar gözlenmiştir. Morfolojinin daha değerlendirilmesi için HRTEM yöntemi kullanılmış ve bahsi geçen karbon zincirlerinin yakından incelenebilmesi sağlanmıştır. Bu yöntemde, karbonlu yapının herhangi bir grafen düzlem içermediği ancak amorf matris içinde kristal yapıda noktalar gözlenmiştir. Bununla beraber, atomlar arası mesafelerde $\simeq 1$ nm kadar sapmalar gözlenmiştir.

Anahtar Kelimeler: Kurum, Brülör, TGA, Koklaşma, RFG

To my precious family and my beloved sweetheart

ACKNOWLEDGEMENTS

I would first like to thank and express my regards to my thesis advisor, dear Assist. Prof. Dr. Feyza Kazanç Özerinç, for her incredibly kind and caring attitude. The door of Assist. Prof. Dr. Feyza Kazanç Özerinç was always open whenever I needed her help. Her useful comments and remarks guided me seamlessly until the end of this thesis study. I would like to appreciate to my examining committee members, Prof. Dr. Ahmet Yozgatlıgil, Assoc. Prof. Dr. M. Metin Yavuz, Assoc. Prof. Dr. Çağlar Sınayuç, and Assoc. Prof. Dr. Murat Kadri Aktaş for their valuable time, evaluation and participation. A special thank goes to my dear lab colleague Duarte Magalhaes who was always there to answer my questions with great pleasure. His endless donorship made me happy and thankful every time. His assistance with experimental trials, corrections in my thesis are gratefully appreciated. I would like to thank Central Laboratory of the Middle East Technical University, for the support they always provided to me about everything. Special thanks go to my family and my sweetheart Ebru İlter, who were supporting me from the beginning of my study to the end of it.

TABLE OF CONTENTS

ABSTRACT v

ÖZ vii

ACKNOWLEDGEMENTS x

TABLE OF CONTENTS xi

LIST OF TABLES xiv

LIST OF FIGURES xv

CHAPTER 1

1. INTRODUCTION 1

1.1. Motivation and Objective 4

CHAPTER 2

2. LITERATURE REVIEW 7

2.1. Pet Coke 7

2.2. Refinery Fuel Gas (RFG) Combustion in Boilers 10

2.3. Soot 11

2.4. Soot Morphology 12

2.5. Soot Formation 15

2.5.1. Effect of Flame Type in Soot Formation 18

2.5.2. Sooting in Gaseous Diffusion Flames 18

2.6. Practical Impact of Soot Formation in Boilers 20

2.7. Thermogravimetric Analysis for Carbonaceous Substances 20

2.8. Morphological, Chemical Composition and Structural Analysis of Carbonaceous Substances 23

CHAPTER 3

3. MATERIALS AND EXPERIMENTAL METHODS 29

3.1. Composition of the Refinery Fuel Gas (RFG) 29

3.2. Soot Sample Collection from Burner Tips 31

3.3. Soot Sample Preparation for Analysis 33

3.4. Experiments for Soot Sample Characterization 37

3.4.1. Experimental Setup 37

3.4.2. Experimental Method 43

3.4.3. Measurement Errors and Uncertainties of Experimental Methods 46

CHAPTER 4

4. RESULTS AND DISCUSSION 49

4.1. Thermogravimetric Analysis of Soot Sample Derived from RFG Combustion 50

4.2. Wire Mesh Reactor Analysis of Soot Sample 56

4.3. Morphology, Chemical Composition and Structure of Soot Sample 57

4.3.1. SEM and EDX Results 57

4.3.1.1 EDX Results of SEM Images 60

4.3.2. HRTEM Results 63

4.3.3. XRD Results 65

4.3.4. RAMAN Results 66

CHAPTER 5

5. CONCLUSION AND FUTURE STUDY 69

5.1. Conclusion 69

5.2. Future Study 70

REFERENCES.....73

APPENDIX

A. Detailed Results.....79

A1. Additional Results of FTIR.....79

A.2. Extended Results of XRD.....80

A.3. Detailed EDX results.....81

A.4. Closeup View of SEM Images.....81

A.5. Closeup View of TEM Micrograms.....82

LIST OF TABLES

TABLES

Table 2.1 Typical properties of green and calcined coke [11][18] 9
Table 2.2 Relative sooting tendency, surface area and number of particles in 1 g of soot formed during pyrolysis of hydrocarbons at 1623 K and soot yield of 60 wt. % [31] 14
Table 3.1 Properties of the refinery fuel gas (RFG) 30
Table 3.2 XRD measurement conditions 46
Table 4.1 Wire mesh experimental conditions and fuel gas soot (FG) sample yields 56
Table 4.2 EDX results of the sample images by scan number 60
Table A.1 Qualitative analysis results of XRD 80
Table A.2 Peak list from XRD data 80

LIST OF FIGURES

FIGURES

Figure 1.1 Shares of global primary energy generation by fuel given as percentage by year [5] 2
Figure 1.2 Energy generation by source in Turkey (2017) [6] 3
Figure 2.1 Sponge Coke [17] 8
Figure 2.2 Shot coke [17]....9
Figure 2.3 Refinery Fuel Gas (RFG) cycle in a refinery [20]....10
Figure 2.4 A. Soot volume fractions in rich-premixed CH_4, CH_4/C_2H_6, CH_4/C_3H_8 and CH_4/n-C_4H_{10} flames as a function of equivalence ratios. The dotted line denotes this arbitrarily chosen fixed soot amount (30 ppb , see text for details), B. Equivalence ratio for soot fraction of 30 ppb as a function of PE [32] 14
Figure 2.5 Designation of soot formation [22]....16
Figure 2.6 Physical and chemical processes in a candle [34] 17
Figure 2.7 Lines of constant soot particle numbers per cm^3 for a laminar diffusion flame [30], [44]. 19
Figure 2.8 TGA traces for different SWNT materials and graphite powder, for comparison. Heating rate 58C/min in Ar:O_2 (92:8,2 v/v) flowing at 100 mL/min [55] 21
Figure 2.9 TGA measurement of the oxidation of natural graphite in air. Heating rate 10 °C/min [56] 22
Figure 2.10 Thermogravimetric analysis of a typical graphite and differential curves at a heating rate of 1 °C/min in air (100 mL/min) [57]....22
Figure 2.11 Scanning electron micrographs of soot obtained from the combustion of kerosene [26]....23
Figure 2.12 X-ray diffraction pattern of soot obtained from the combustion of kerosene [26] 24

Figure 2.13 RAMAN of amorphous carbon [58] 25
Figure 2.14 RAMAN spectra of sooth obtained from the combustion of kerosene [26] 25
Figure 2.15 TEM images of young and mature ethylene and benzene soot [59] 26
Figure 2.16 HRTEM images of methane (a–d) and ethylene soot (e–h) [59] 26
Figure 2.17 HRTEM images of soot for ethanol droplet burning in 30% O_2 in Ar at 0.24 MPa (left: 1.6 mm ethanol droplet, right: 2.2 mm ethanol droplet) (solid white bar represents 5 nm) [61] 27
Figure 2.18 Printex U HRTEM micrograph 27
Figure 2.19 Typical examples of TEM images of soot particles taken at 2.3 atm, 5.4 atm, 7.1 atm, and 10 atm. Solid bars on the images represent 100 nm 28
Figure 3.1 Burner tips marked on a sample burner design 31
Figure 3.2 Renewed burner tips 32
Figure 3.3 Fuel gas soot (FG) sample gathered from the burner tips 34
Figure 3.4 Grinding in mortar 34
Figure 3.5 Process scheme taken from Honeywell UOP [64] 35
Figure 3.6 Axens CCR reforming process [65] 35
Figure 3.7. TGA and FTIR setup 38
Figure 3.8 SEM Visual [67] 40
Figure 3.9. Wire mesh reactor setup 41
Figure 3.10 Characteristic temperatures during non-isothermal TGA experiments (T_v – decomposition temperature; T_i – ignition temperature; T_p – peak temperature; T_e – end temperature) 44
Figure 3.11 IR Spectrum of CO_2, CO, SO_2 and H_2O 45
Figure 4.1 Characteristic combustion temperatures for non-isothermal TGA 51
Figure 4.2 TG and DTG profiles for the non-isothermal combustion of the fuel gas (FG) soot sample at a heating rate of 15 ºC/min (5 mg, 75-106 µm particle size) 51
Figure 4.3 TG and DTG profiles for the isothermal combustion of the fuel gas soot (FG) sample at 700 ºC (5 mg, 75-106 µm particle size) (2 repetitions) 52

Figure 4.4 DTG profile and FTIR absorbance spectrum of CO_2 of the isothermal combustion of the 75-106 µm fuel gas soot (FG) sample at 700 ºC 54
Figure 4.5 DTG profile and FTIR absorbance spectrum of CO of the isothermal combustion of the 75-106 µm fuel gas soot (FG) sample at 700 ºC 55
Figure 4.6 SEM images of 0-75 µm particle sized fuel gas soot (FG) sample 58
Figure 4.7 SEM images of a 75-106 µm particle size of fuel gas soot (FG) sample 59
Figure 4.8 Selected area and results for EDX scans #1 for 75-106 µm particle sized fuel gas soot (FG) sample 60
Figure 4.9 Selected area and results for EDX scan #2 for 75-106 µm particle sized fuel gas soot (FG) sample.....61
Figure 4.10 Selected area and results for EDX scan #3 for 75-106 µm particle sized fuel gas soot (FG) sample 61
Figure 4.11 Selected area results for EDX scan #4 for 75-106 µm particle sized fuel gas soot (FG) sample 62
Figure 4.12. HRTEM micrograms of FG soot sample.....63
Figure 4.13. HRTEM micrograms of FG soot sample (A: indicates ordered region of carbon atoms, B: amorphous region) (solid line corresponds to 5 nm) 64
Figure 4.14 XRD raw data peak comparison with graphite-2H peaks 65
Figure 4.15 XRD data with graphite-2H peaks (simplified view).....66
Figure 4.16 RAMAN of the fuel gas soot (FG) sample @532 nm laser edge.....67

CHAPTER 1

INTRODUCTION

The increase in the energy consumption in parallel with the population growth over the recent years has gained wider importance in terms of the consequences it has and may create. Having efficiency as a main concern for the engineers in the field on one side, rapid developments in technology increased the demand for energy and its consumption.

This increase in the energy demand has led governments to seek for cheaper and more efficient fuels and energy sources. Along with its accessibility and availability, natural gas is one of the cheapest energy sources with 68 £/MWh (combined cycle gas turbine) compared to 171 £/MWh of coal, according to BEIS (Department of Business, Energy and Industrial Strategy of UK) [1].

In addition to its cheapness, natural gas is also more efficient and environmentally friendly compared to coal. Supportively, its CO_2 emission is only 59% of coal and 72% of oil relatively when it is burned [2]. Moreover, methane, which forms the biggest part of the composition of natural gas [3], has the least yield sooting index among other hydrocarbons [4].

Figure 1.1 shows the global tendency for natural gas with an increase by 8.4 percent point from 1965 to 2017.

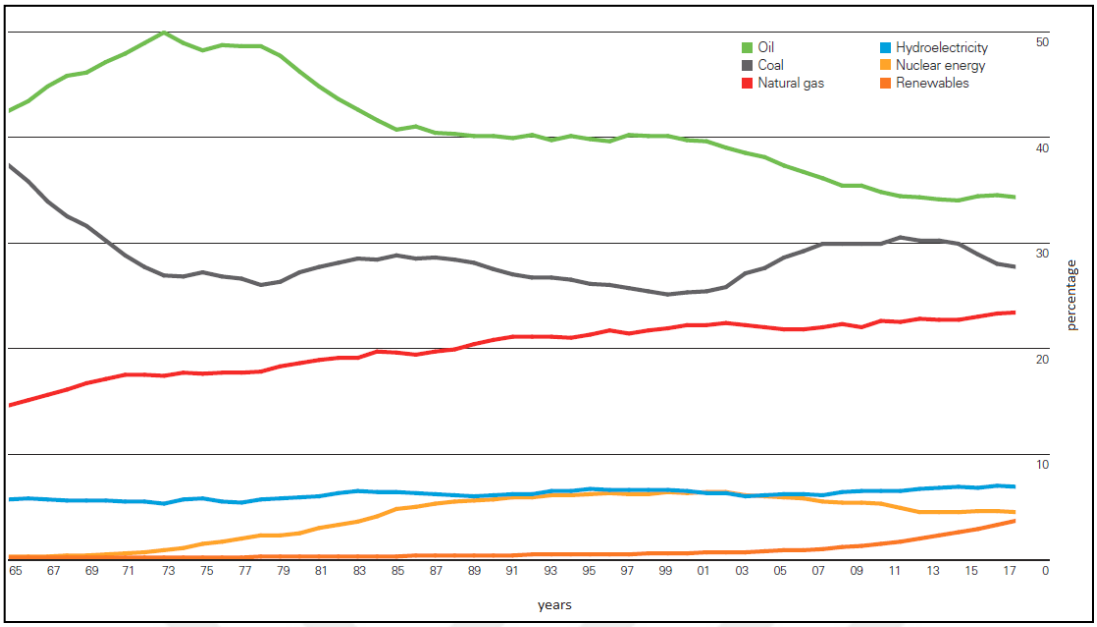

Figure 1.1 Shares of global primary energy generation by fuel given as percentage by year [5]

Natural gas consumption for energy generation trends for Turkey appears similar to the global trends with an approximate 5 percent point increase from 2016 to 2017. Changing the figures, this increase has gained the biggest pie to natural gas with 37%, followed by coal with 33% as shown in Figure 1.2.

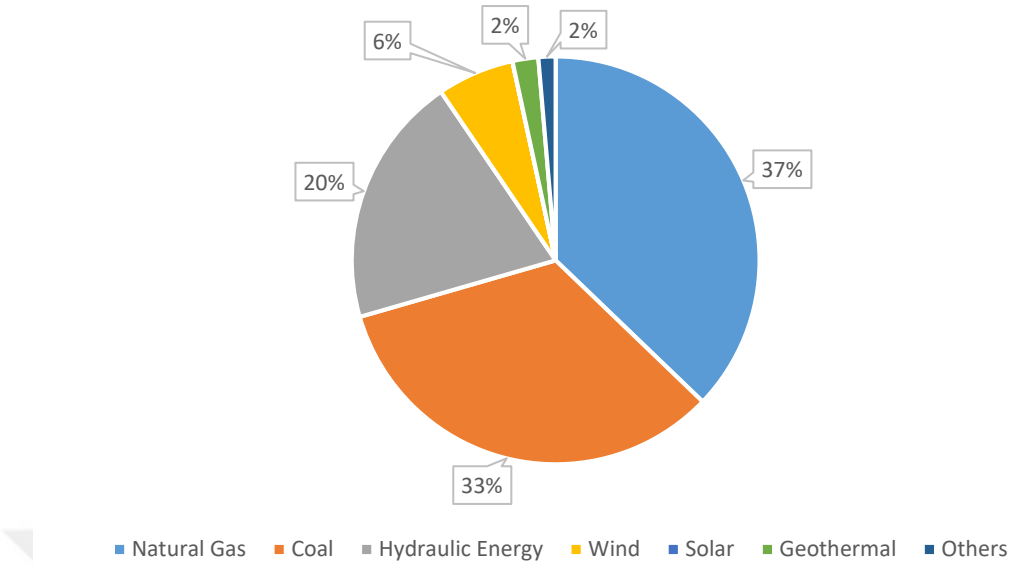

Figure 1.2 Energy generation by source in Turkey (2017) [6]

Since these fuels can be used to generate heat as well as electricity, plants can utilize solid, liquid or gas fuels in their industrial furnaces for this purpose. Though all these three options bring along their own advantages and disadvantages, natural gas appears to stand out due to its cost effectiveness, efficiency, environmentally friendly composition and ease of operation.

However, despite being regarded as one of the most environmentally friendly fossil fuels, natural gas might have an indirect adverse effect because of the fact that it may generate such by-products as soot, which is also a common by-product of almost all fuels. Soot is not desired because of the industrial purposes for diminishing the efficiency of the devices that they are generated inside and rising concerns of exceeding stack emissions.

In oil refineries, it is not uncommon to mix the excess process gasses with natural gas to produce Refinery Fuel Gas (RFG). RFG is a gaseous mixture mainly consisting of mostly more than 85% methane, hydrogen, light hydrocarbons and other hydrocarbons

of ethane, propane, butane, etc. RFG can be used in boilers and process heaters throughout the refinery [7].

In operating the boilers in industries, soot and scale problem constitutes one of the most important issues to address [8]. If it reaches 10 mm of thickness on heater tubes, the soot may result in energy losses as high as a 10%. Moreover, the conversion of initial 10-20% of the fuel in diesel engines into soot and reducing combustion efficiency, it also affects our daily lives [9].

In this scope, the present work addresses one of the detrimental issues during operation of RFG fueled burners through an in-depth investigation on the elimination of industrial burner clogging caused by soot formation. To do this, chemical, thermal and morphological properties of soot is studied.

1.1. Motivation and Objective

Motivation is driven by the fact that operational safety and efficiency are the most important issues in energy industry which are disrupted because of the soot, despite having been underrated so far. Usually, clogged burners are dismantled from the furnace and cleaned mechanically. This study focuses on extending these maintenance intervals or completely remove the need for it by investigating properties of soot and proposing a solution to it.

There are various analysis methods in literature including Thermogravimetric Analysis (TGA), Scanning Electron Microscope (SEM), High-Resolution Transmission Electron Microscopy (HRTEM). Combining different experiments and analysis methods, this study gives an opportunity to the reader to have separate results from the same soot sample. The motivation of the thesis in to bring together a variety of analysis and experiments to give an in-depth insight of morphology and

thermochemical properties of soot. These experiments were done to gain a comprehensive insight on elimination methods of soot in industrial boilers.

Chemical, morphological and combustion characteristics of soot were examined in this thesis. Following are done in this thesis: a TGA coupled with Fourier Transform Infrared Spectrometer (FTIR) to reveal the thermal reactivity of soot, a Wire Mesh Reactor (WMR) to inspect behavior of soot under high heating rates, HRTEM and SEM are used for imaging the specimen with Energy Dispersive X-ray (EDX) to analyze the contents of it, X-ray powder Diffraction (XRD) and RAMAN to inspect molecular structure and chemical composition of soot. Soot is sometimes confused with petroleum coke and an introductory part to identify the coke and the difference in between is given.

CHAPTER 2

LITERATURE REVIEW

2.1. Pet Coke

Crude oil is a mixture (emulsion) that contains a variety of long hydrocarbon compounds. In petroleum refineries, this mixture is processed to extract these hydrocarbon compounds and further process them to obtain products that satisfy the specifications of the fuel types.

A refinery with an average complexity will process 65-72% of the crude oil into light and middle distillates such as LPG, gasoline, jet fuel and diesel and 28-35% into the fuel oil products. [10] Fuel oil products are not being demanded as much they were in 1980s, and the higher a refinery produces fuel oil the less it is profitable because of this. Therefore, refineries try to re-process fuel oil into lighter products.

These processes take place in “coker” units which are built to upgrade the “residuum” into gasoline and middle distillate fuels. This will improve the limited refining percentage of crude oil and lower the amount of “residuum”, which can be thought as inconsumables with a low added value.

There are mainly three different types of coker units, which are called *delayed coker, flexi coker* and *hid coking*. The most commonly utilized one is delayed coker units. Cokes are classified depending on their physical and chemical properties and will be discussed in the next section [11].

After refining crude oil in refineries, there is a final processed product is produced, which is called petroleum coke. It is a concentrated carbon solid residue, which is

abbreviated as “pet coke” [12]. Pet coke is obtained from a process called thermal cracking, which breaks the long hydrocarbon chains into shorter ones [13].

The coke produced in refineries is called “green coke”. Green coke, which means unprocessed coke, can be used as fuel and can be further processed to improve its properties matching the demanded properties in the industry such as increasing its density and calorific value [14]. The following pet coke types are formed regarding the feedstock and operation parameters during the production: [15]

- Green Coke (raw coke) is a fuel-grade unprocessed coke formed in refineries,
- Calcined Coke is the heat-treated green coke at around 1200-1350 °C. At such high temperatures, the moisture and volatiles are extracted, and the density of the coke is further increased. This allows it to be used in aluminum industry for example, in production of welding rods. Calcined coke can be classified as follows:
    - Needle Coke is a high-grade coke mostly used in steel industry which has a good electrical conductivity.
    - Sponge Coke is a regular coke generally used as anode production, which is dull and black. It is physically a porous material.
    - Shot Coke is produced from heavy feedstock, which has a spherical form [16].
    - Honeycomb Coke is an intermediate grade coke, which has ellipsoidal pores and has a lower electrical conductivity than needle coke.

Figure 2.1 Sponge Coke [17]

Figure 2.2 Shot coke [17]

Table 2.1 Typical properties of green and calcined coke [11][18]

	Green	**Calcined**
Sulfur (wt%)	2.5-5.5	1.7-3.0
Ash (wt%)	0.1-0.3	0.1-0.3
Nickel (ppm)	-	165-350
Vanadium (ppm)	200-400	120-350
Volatile matter (wt%)	9-12	<0.25
Bulk density (g/cm3)	-	0.8
Real density (g/cm3)	-	2.06

As it can be seen in Table 2.1, calcination process is used to remove the volatiles, some sulfur content and hydrogen in order to increase density and electrical conductivity. Therefore, calcined cokes can be used as anodes for aluminum production [18].

2.2. Refinery Fuel Gas (RFG) Combustion in Boilers

Refinery units often generate excess gasses that could be used as fuel supply. These fuel gas streams from different refinery units to a common mixing point and delivered back to the units from there (see Figure 2.3). Since plants change operation parameters daily to meet production demands and specifications, the excess gasses they produce may change in contents. Therefore, components of fuel gas could change from one day to another [19].

Refinery fuel gas is a homogenous gaseous mixture of light hydrocarbons, hydrogen, methane and some other species produced in refinery. It can also be mixed with natural gas and used afterwards [7]. Mixing the RFG homogenously is crucial since it plays an important role in combustion performance. Changing the homogeneity, changes stability of burner, heat flux, heat transfer efficiency, emission controls by affecting the calorific value of the mixture. In using fuel gas, such a problem like liquid phase existence in the mixture could also be encountered. This liquid phase is not desired since it promotes soot formation in the burners and should definitely be eliminated by using filtration methods [19].

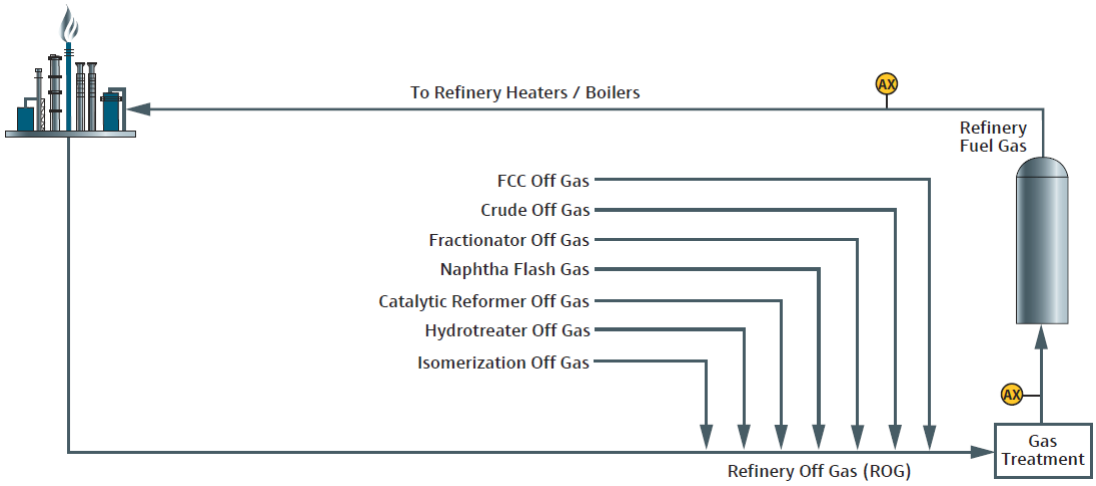

Figure 2.3 Refinery Fuel Gas (RFG) cycle in a refinery [20]

2.3. Soot

Combustion-generated particles are called soot [19]. Soot is different from coke, as it forms under uncontrolled environments.

Soot is basically small submicron carbonaceous particles commonly seen in combustion and pyrolysis of hydrocarbons. Soot could be observed in most combustion systems from a burning candle to sophisticated industrial burners [21].

In theory, if the conditions are ideal, stoichiometric hydrocarbon combustion products are CO_2 and H_2O. Under this condition maximum chemical energy is transferred into maximum thermal energy [22].

Although having stoichiometric combustion is desired, in practical operations, it is mostly a theoretical utopia. If the conditions are off the stoichiometric combustion, other by-products such as carbon monoxide, hydrogen, some hydrocarbons and soot can appear in the right-hand side of the combustion equation. This will affect efficiency and cause some undesired consequences which will be discussed later on [22]. Conditions of combustions taking place in industrial furnaces are paid utmost attention since the flue gas emissions are limited by law-makers and controlled by regulators.

$$\text{hydrocarbon} + \text{oxygen} \rightarrow \text{carbon dioxide} + \text{water}$$

$$CH_4(g) + 2\ O_2(g) \rightarrow CO_2(g) + 2\ H_2O(g)$$

Soot could be found in every kind of system that a combustion is happening, especially in combustion systems with diffusion flames. Soot particles first appear in very small amounts (diameter of a few Angstroms), and subsequently tend to group up and stick together to form aggregates that look like chains of carbon atoms or branch like structures. It should be known that although there are many factors affecting soot formation, the general structure is very similar to each other of the soot aggregates

between the combustion systems with varied pressure, temperature, fuel type and mixture rates [23].

Particles of soot are also very active in terms of taking in other materials into their structure. This means mature soot particles may include some other substances in them but if the steps of soot formation were observed, immature particles would look very similar as it was mentioned in the previous paragraph [23].

As soot is almost a fully carbonaceous substance, it could be thought that it could be oxidized relatively easily. However, removing soot from the combustion chamber is not easy, because this chemical reaction is comparatively slower than the oxidation of actual fuel molecules, for a diffusion flame [23].

Although the existence of soot in combustion mechanisms is very well known, its chemical formation mechanism is still not fully understood because of the fast-parallel reactions occurring at the same time. Formation mechanism of soot is widely researched, and many models have been proposed [9].

2.4. Soot Morphology

Soot is matte black and looks like pseudospherical particles that sticked together to form chain like structures. Immature soot particles look alike not depending on what conditions it was generated, although mature ones may absorb other by-products generated by the combustion process itself. These by-products could be polycyclic aromatic hydrocarbons (PAH), atomic hydrogen, or other substances.

Soot will also be addressed from the morphological point of view. It is made of aggregates, looking like and made from smaller spherical particles. These particles are ranging from 10 to 500 nm in size. Also these aggregates could be formed from multiple particles [24]. Easiest way to see particles which have this scale of size is to

observe the samples under electron microscope. Many studies have been made in order to observe what soot particles look like and what their morphology is [25], [26], [27].

According to Ban et al. internal structure of soot particles can be considered as an arrangement of bent carbon layers which follow shape of particle surface, having many dislocations and lattice defects. These defects and interplanar spacing causes a very low density (lower than 2 g/cm^3) [23]. Young soot particles which are in growth phase have shown much stronger electron paramagnetic resonance (EPR/ESR) signals than fully developed ones [28], [29].

Sooting tendency of some of the hydrocarbons are given below. Tendency increases from paraffins to mono- and diolefins, benzenes and naphthalenes [30]. Note that the tendency of some hydrocarbons is much higher than others so even though they do not exist as higher proportions in the mixture, they could have more effect on the result.

Table 2.2 Relative sooting tendency, surface area and number of particles in 1 g of soot formed during pyrolysis of hydrocarbons at 1623 K and soot yield of 60 wt. % [31]

Hydrocarbon	Surface area, A (m^2/g)	Number of particles in 1 g of soot, N_0 (g^{-1})	Sooting tendency $N_0/N_{0(CH4)}$
Methane	22.9	$4.2x10^{14}$	1
Ethylene	36.6	$1.7x10^{15}$	4
Acetylene	44.8	$3.2x10^{15}$	7.6
Diacetylene	84	$2.1x10^{16}$	50
Benzene	40.4	$3.1x10^{15}$	7.4
Toluene	40.4	$2.3x10^{15}$	5.5
Xylene	36.1	$1.7x10^{15}$	4
Naphthalene	110	$4.7x10^{16}$	112
Anthracene	102	$3.8x10^{16}$	91
Pyrene	95.4	$3.1x10^{16}$	74

Visser et al. [32] suggests that at a constant equivalence ratio, adding higher alkanes into methane increases the soot generated in rich pre-mixed mixtures of CH_4, C_2H_6, C_3H_8 and C_4H_{10} (Figure 2.4).

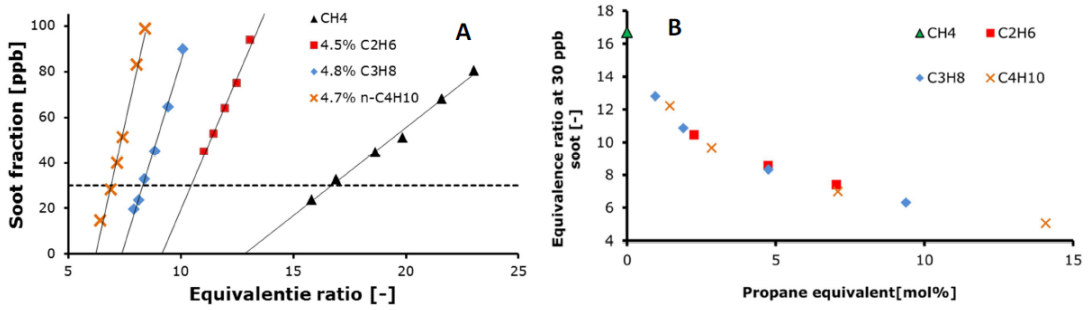

Figure 2.4 A. Soot volume fractions in rich-premixed CH_4, CH_4/C_2H_6, CH_4/C_3H_8 and CH_4/n-C_4H_{10} flames as a function of equivalence ratios. The dotted line denotes this arbitrarily chosen fixed soot amount (30 ppb , see text for details), B. Equivalence ratio for soot fraction of 30 ppb as a function of PE [32]

2.5. Soot Formation

Soot formation is mainly due to incomplete combustion. It can happen when there is fuel-rich mixtures in the near burner region, insufficient atomization of fuel oil causing larger fuel droplets in combustion chamber, high moisture content in the fuel, erratic feeding of solid fuels and dripping burner [8]. Soot is commonly formed when combustion is fuel rich to the point that conditions allow condensation and polymerization of the fuel [21].

$$C_xH_y + (x+y/4)\ O_2 \rightarrow x\ CO_2 + y/2\ H_2O$$

Under stoichiometric conditions, maximum of chemical energy is transformed into maximum thermal energy [22].

In combustion devices (combustion engines, industrial furnaces, gas turbines…) conditions deviate from the stochiometric case locally. When this happens, other products of incomplete combustion appear such as carbon monoxide, hydrogen, some hydrocarbon species and soot [22].

The soot formation process is considerably complex. It can be seen as a gaseous-solid phase transition. It includes the formation and growth of large PAH's. The transition of these into solid particles and the coagulation of smaller first-born particles into aggregates and pick up of gaseous components into their structure with formation of larger chunks of soot. Given below in Figure 2.5 is the summary and visualization of stages of soot formation based on current hypotheses [22].

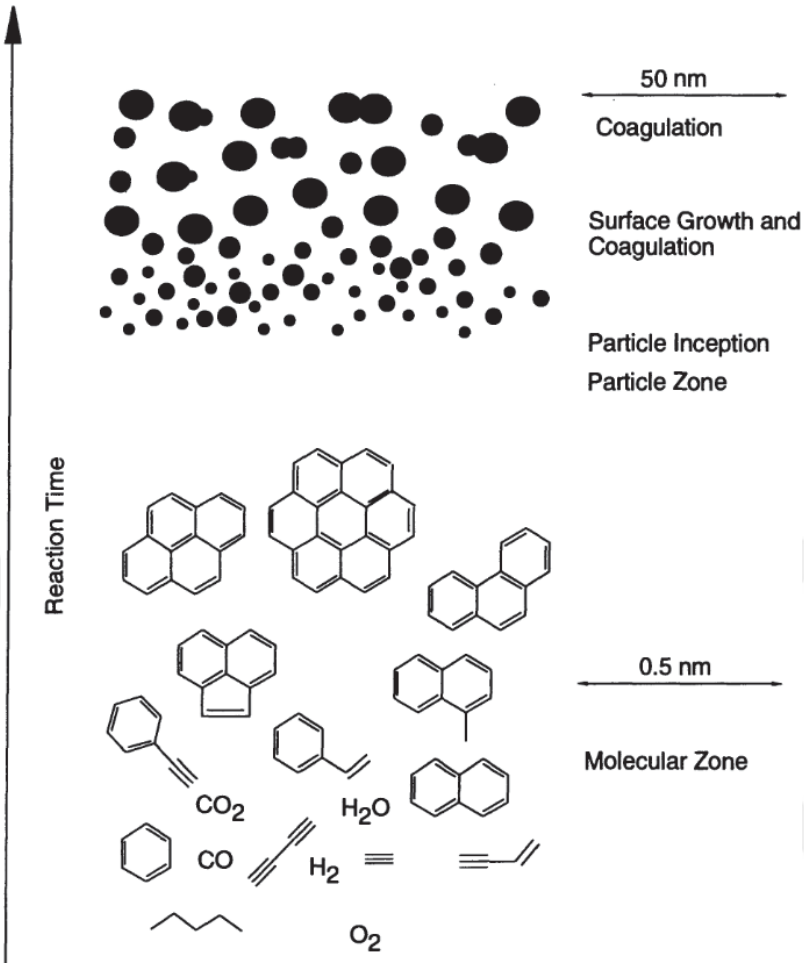

Figure 2.5 Designation of soot formation [22]

A basic illustration of a candle flame is given in Figure 2.6 to point out the domains where soot forms.

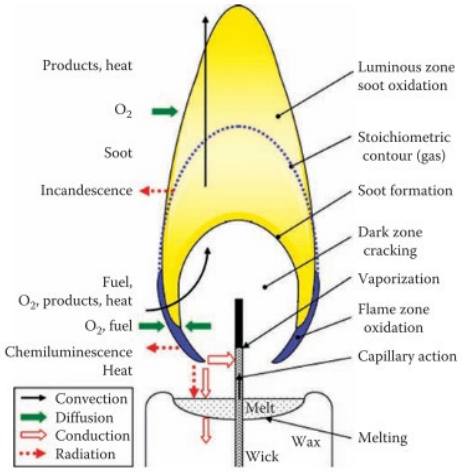

Figure 2.6 Physical and chemical processes in a candle [34]

In heavy industry, fired heaters operate around 1000°C to 2300°C. As in every other combustion reaction taking place, soot formation is also a concern in these industrial devices. Comparing these to other combustion types, such as in a candle flame or in an internal combustion engine, soot particles that are initially formed are not much different than the others (around 20-50 nm) [35]. It should be noted that ratio of soot generation to actual amount of carbonaceous fuel burning is very low. Soot formation generally comes together with other unsaturated hydrocarbons, polycyclic aromatic hydrocarbons (PAH) and other substances. Some of these substances can live in these temperature ranges [36] and exist after the combustion with solid carbons. They can even condense and adsorb on soot particles [23].

Leung et al. [37] suggests a 111 forward step reaction for soot mechanism. Leung et al. divides soot lifespan into 4 terms, soot nucleation, surface growth, particle coagulations, and destruction via combustion. He also suggests that combustion state in terms of concentration of fuel versus the oxidizer is having a great impact on the sooting characteristics. Also, sooting is dependent on the breakdown path of the fuel and by products appearing inter combustion steps [37].

Soot formation in its entirety has not yet been fully understood.

2.5.1. Effect of Flame Type in Soot Formation

When the combustion takes place a flame is generated and the soot formation tendency is affected by whether the combustion is premixed or non-premixed [9].

In non-premixed combustion, fuel and oxidizer are fed into the combustion chamber separately. Because of that, mixing in combustion is dependent on the diffusion of oxidizer and fuel on the flame surface. Flame in non-premixed combustion is therefore called diffusion flame [34].

In premixed combustion, fuel and oxidizer are mixed together before being delivered to the combustion zone. This type of combustion is not preferred as much as non-premixed combustion in industrial furnaces [38].

Soot formation tendency increases with an increase in flame temperature in non-premixed (diffusion) flames. On the other hand, in premixed flames, soot formation tendency decreases with increasing flame temperature [39].

Böhm et al. [40] suggests that in premixed flames, increasing pressures rise the sooting threshold and thus the volume of soot is increased [41],[42],[43]. The researchers also confirm that in premixed flames, increasing temperature decreases the soot volume fraction [40].

2.5.2. Sooting in Gaseous Diffusion Flames

If fuel and oxidizer reach to the combustion chamber flowing through separate inlets, and combustion is governed by diffusion or as called “mixing controlled”, a diffusion flame is taking place. Since it is safer to operate compared to premixed flames, most combustion systems use diffusion flames. It can be seen that in such systems, it is

really hard, almost impossible to expect C/O ratio to stay below the critical limit in every domain around the flame [30].

Aforementioned phenomena could be observed by taking C_2H_4 as fuel and supplying it into air from a circular burner. As the flow speed gets increased, the flame will look like and change from a Bunsen burner flame, which only a little amount of soot luminosity would be seen, into a flame which has yellow luminosity, lastly to a higher flame which from a point, soot starts to emit and become smoke [30].

Wagner et al. [30] add that the luminosity of a flame can give an impression of the soot distribution. Referring to Kunugi and Jinno et al. [44], in a laminar diffusion flame, along the centerline, soot particles, from burner port, about 1 cm and above increases drastically and approaches a maximum at about 60% of the flame height with $3x10^8$ particles/cm^3 (Figure 2.7). This behavior is typical for diffusion flames. "The soot concentration maximum in diffusion flames occur at a place, where the rate of particulate formation equals its rate of oxidation" [30].

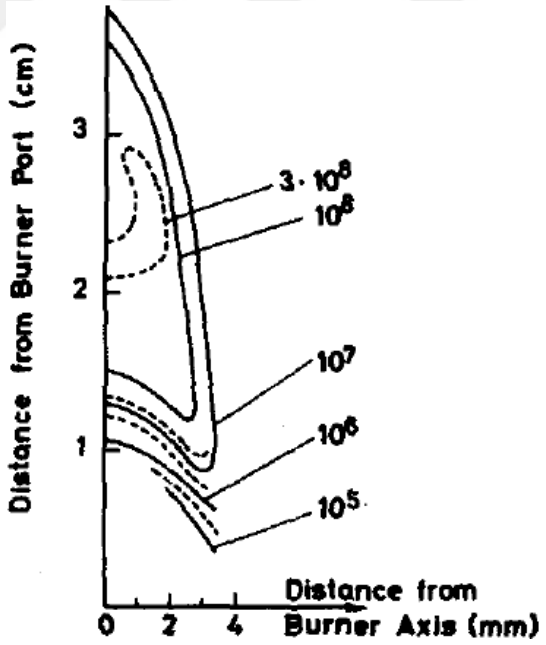

Figure 2.7 Lines of constant soot particle numbers per cm^3 for a laminar diffusion flame [30], [44].

2.6. Practical Impact of Soot Formation in Boilers

Studies on soot are done due to the following negative consequences of soot formation. When soot particles stuck on the outer surface of heater tubes, heat transfer from combustion chamber to the products flowing through heater tubes decrease, resulting in increased stack temperatures [45].

Even though technical consequences of soot formation are the primary motivation for most, health risks and pollution are also an important case. Since soot particles contain molecules of polyaromatic hydrocarbons, they are harmful for human health causing cancer and respiratory diseases [22], [46].

In fact, according to the World Health Organization, soot, as a particulate matter, is a pollutant [47]. Air pollution is largely caused by particulate matters caused by diesel engines and combustion by-products of fuels used in power plants [48].

This thesis differentiates from the literature by merging a wide number of experiment and analyses together and giving readers an opportunity of observing and comparing soot with these methods (TGA, FTIR, RAMAN, SEM, EDX, XRD, HRTEM, Wire Mesh) unlike any other source in literature.

2.7. Thermogravimetric Analysis for Carbonaceous Substances

Thermogravimetry is used widely on carbonaceous substances [49], [50], [51], [52], [53], [54].

B. Li et al. [49] studied TGA and FTIR of a coke sample developed on a catalyst. CO and CO_2 evolutions are measured during the TGA.

S. Lebedkin et al. [55] studied characterization of single walled carbon nano tubes (SWNT) with diameters from 2 to 5.6 nm by thermogravimetry and compared the results with graphite powder TGA. The conditions used in the study of S. Lebedkin et al. [55] are 5 ºC/min heating rate in Ar:O_2 (92:8,2 v/v) flowing at 100 mL/min. The graphite powder TGA done (see Figure 2.8) in the study of S. Lebedkin et al. [55] is completely burnt out.

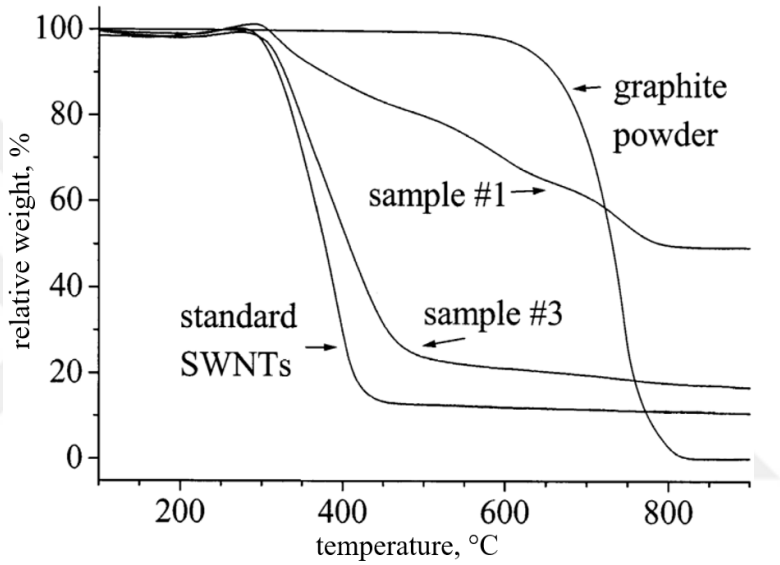

Figure 2.8 TGA traces for different SWNT materials and graphite powder, for comparison. Heating rate 58C/min in Ar:O_2 (92:8,2 v/v) flowing at 100 mL/min [55]

W. Jiang et al. [56] studied oxidation of natural graphite by TGA and results are shown in Figure 2.9. It can be seen that ~100% of the each specimen is burned at the end of the TGA [56].

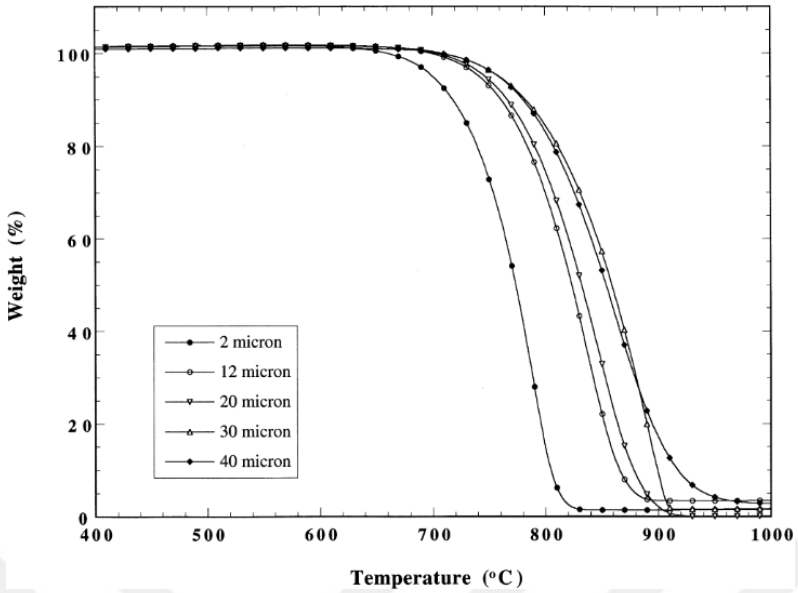

Figure 2.9 TGA measurement of the oxidation of natural graphite in air. Heating rate 10 °C/min [56]

Pang et al. [57] studied the oxidation of carbon nanotubes and nanoparticles with TGA and compared the results with graphite TGA (Figure 2.10) at a heating rate of 1°C/min. Peak combustion rate took place at 645 °C. The graphite specimen is completely burned out in the study of Pang et al. [57].

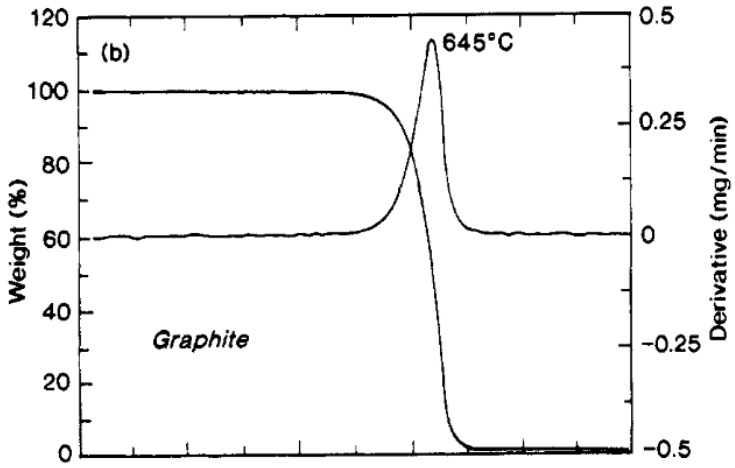

Figure 2.10 Thermogravimetric analysis of a typical graphite and differential curves at a heating rate of 1 °C/min in air (100 mL/min) [57]

2.8. Morphological, Chemical Composition and Structural Analysis of Carbonaceous Substances

In this section literature background of SEM, XRD, TEM and RAMAN techniques are presented.

SEM

Dikio et al. [26] studied SEM of soot from kerosene. Diameters of carbon nanospheres produced from kerosene are about 0.3 μm. Result of the study can be evaluated from Figure 2.11.

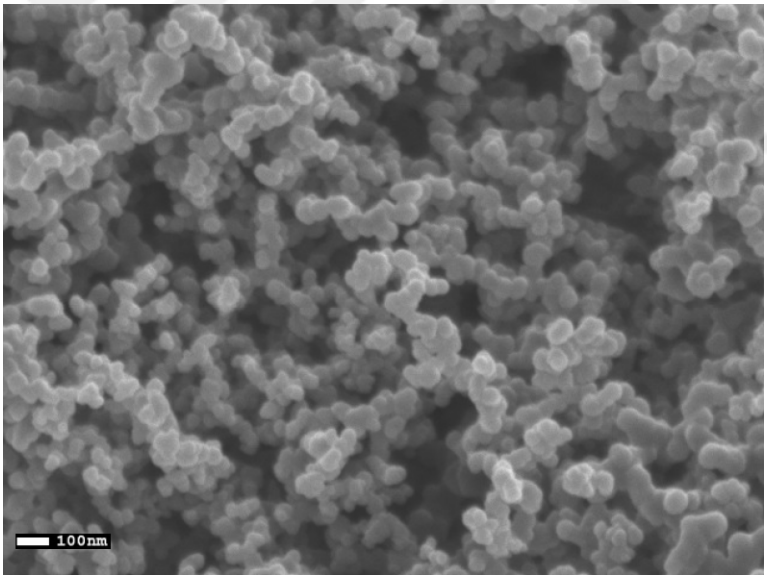

Figure 2.11 Scanning electron micrographs of soot obtained from the combustion of kerosene [26]

XRD

Dikio et al. [26] studied XRD of soot from kerosene. Peaks of XRD can be observed in Figure 2.12 and are at 23.68 and 42.33 2θ degrees.

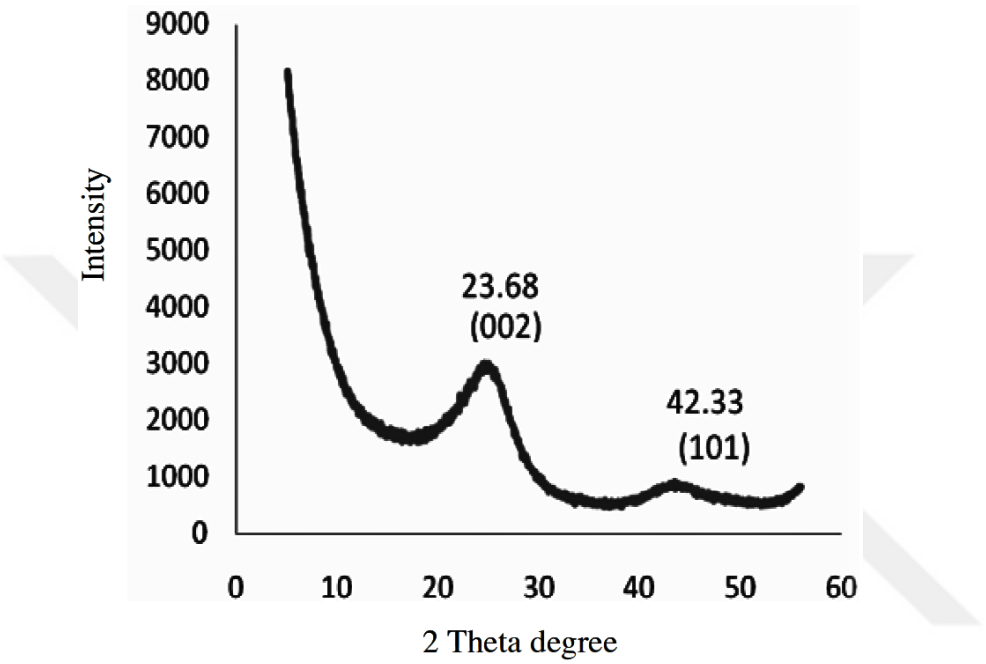

Figure 2.12 X-ray diffraction pattern of soot obtained from the combustion of kerosene [26]

RAMAN

Dychalska et al. [58] studied diamond layers synthesized with Hot Filament Chemical Vapor Deposition method (HF CVD) with amorphous carbon admixture by RAMAN scattering spectroscopy and compared results with RAMAN of amorphous carbon (Figure 2.13).

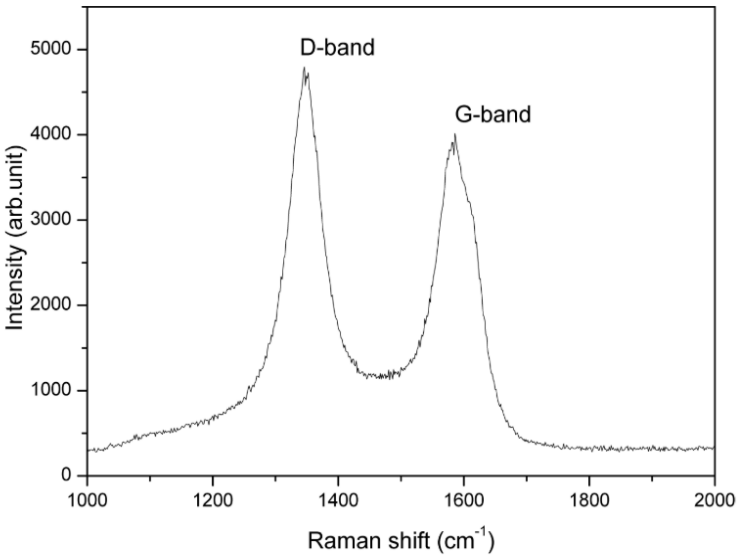

Figure 2.13 RAMAN of amorphous carbon [58]

Dikio et al. [26] studied RAMAN of soot from kerosene. Peaks of the result are at 1330.34 and 1583.88 cm^{-1} (Figure 2.14).

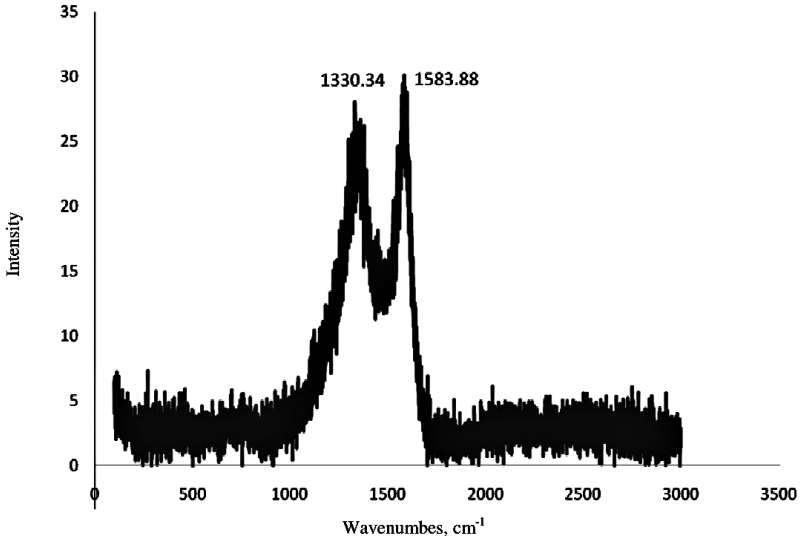

Figure 2.14 RAMAN spectra of sooth obtained from the combustion of kerosene [26]

HRTEM

M. Alfè et al. [59],[60], studied HRTEM images of soot sampled from methane, ethylene and benzene premixed flames burning in fuel rich conditions (Figure 2.15 and Figure 2.16.)

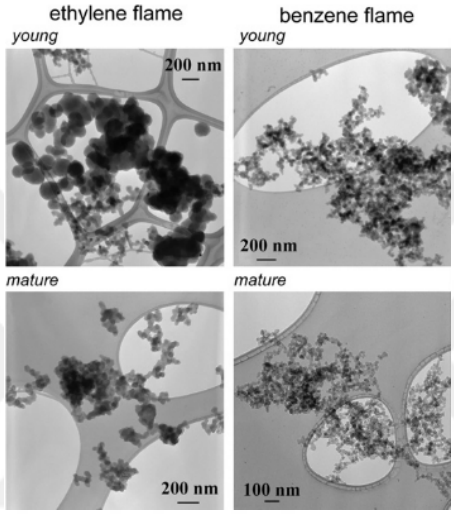

Figure 2.15 TEM images of young and mature ethylene and benzene soot [59]

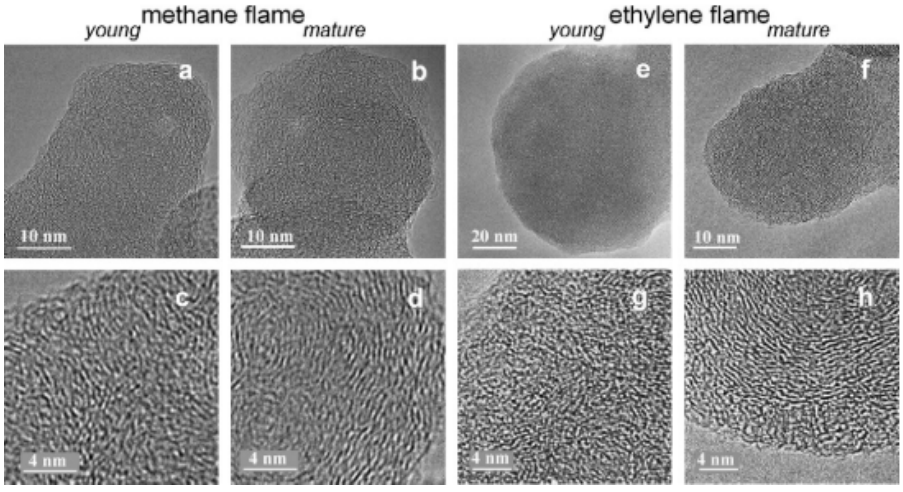

Figure 2.16 HRTEM images of methane (a–d) and ethylene soot (e–h) [59]

Park et al. [61] studied the nanostructure of soot particles collected from spherically symmetric ethanol droplet flame and analyzed HRTEM images (Figure 2.17).

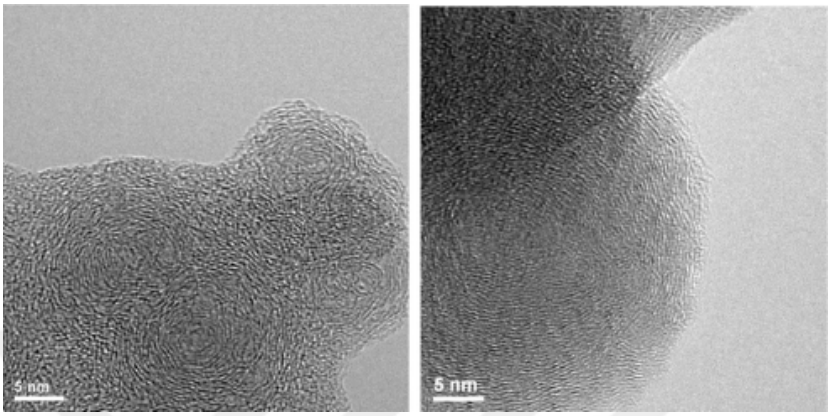

Figure 2.17 HRTEM images of soot for ethanol droplet burning in 30% O_2 in Ar at 0.24 MPa (left: 1.6 mm ethanol droplet, right: 2.2 mm ethanol droplet) (solid white bar represents 5 nm) [61]

Castoldi et al. [62] studied TEM of soot (Printex U) to observe the effect of potassium on the oxidation process which can be seen in Figure 2.18.

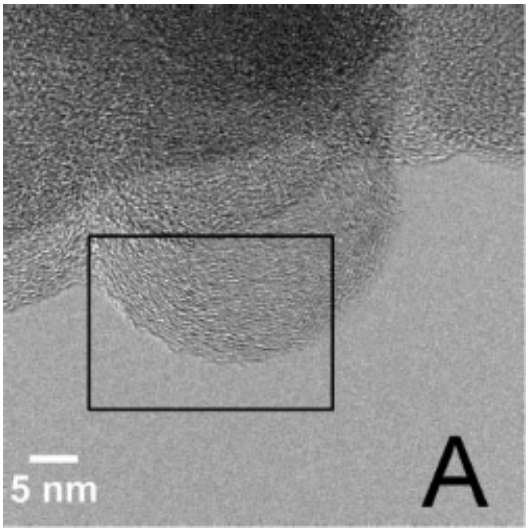

Figure 2.18 Printex U HRTEM micrograph

A. M. Vargas et al. [63] studied TEM images of pressure dependence of primary soot particles as shown in Figure 2.19.

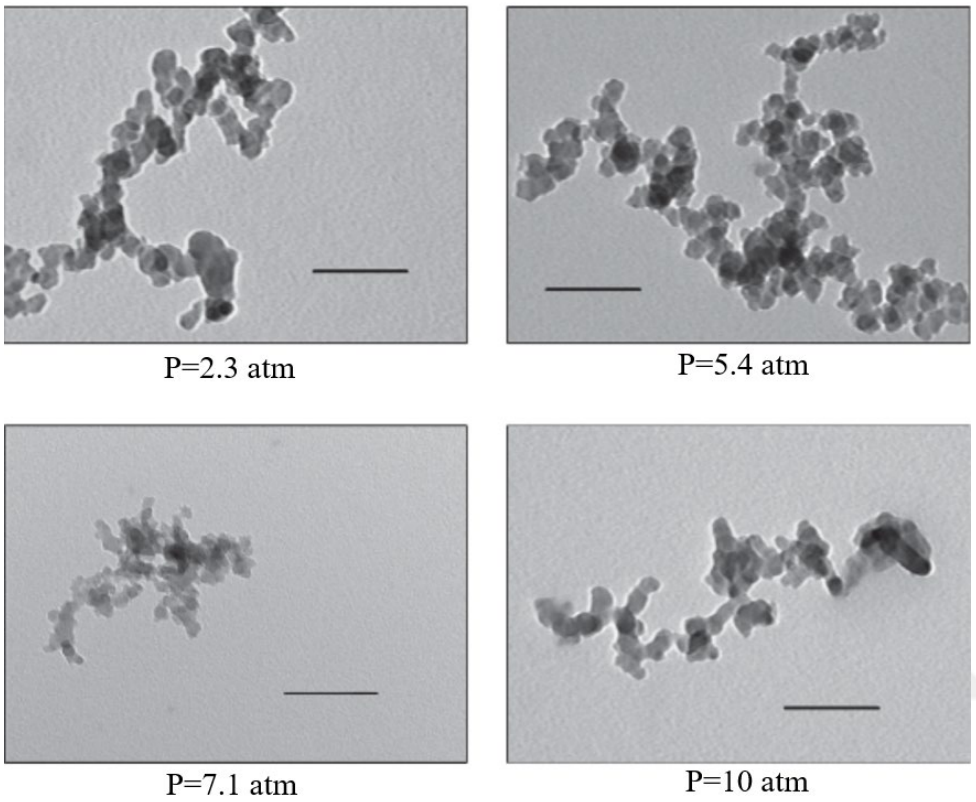

Figure 2.19 Typical examples of TEM images of soot particles taken at 2.3 atm, 5.4 atm, 7.1 atm, and 10 atm. Solid bars on the images represent 100 nm

CHAPTER 3

MATERIALS AND EXPERIMENTAL METHODS

This section explains technical details of the refinery fuel gas (RFG) (i.e. the predecessor of the collected sample), as well as the methodologies for FG soot sample collection, and preparation. An overview of the experimental setups used to investigate the sample collected is also given. Specific parameters of the experiments are explained in detail, and their opting reasons are discussed. A thermogravimetric analyzer (TGA) coupled with Fourier-transform infrared spectroscopy (FTIR), and wire mesh reactor (WMR) are used to inspect the contents and reactivity of the sample. Moreover, scanning electron microscopy (SEM), energy dispersive X-ray (EDX), X-ray diffraction (XRD), RAMAN and high-resolution transmission electron microscopy (HRTEM) techniques are used to have a better insight of the sample morphology-wise.

3.1. Composition of the Refinery Fuel Gas (RFG)

The refinery fuel gas was taken from the companies' live lines and analyzed to get the contents. Represented in Table 3.1 is the gas composition of RFG. As it can be seen from the data, 90% of RFG is composed of flammable carbonaceous content. Specifically, the RFG is mostly composed of methane (62% vol.) and hydrogen (25% vol.).

Table 3.1 Properties of the refinery fuel gas (RFG)

RFG Composition	**Gas composition**	
	% Vol	**% wt**
H_2S	0.004	0.01
H_2	24.61	3.03
CH_4	61.98	60.69
C_2H_6	4.43	8.13
C_2H_4 (Ethylene)	-	-
C_3H_8	3.71	9.99
C_3H_6 (Propylene)	-	-
C_4H_{10}	3.63	12.88
C_4H_8 (Butylene/Isobutylene)	0.01	0.03
C_5+	0.82	3.79
N_2	0.71	1.21
CO	-	-
O_2	0.05	0.10
CO_2	0.05	0.13

3.2. Soot Sample Collection from Burner Tips

The soot sample is collected from a burner of the pre-heater furnace of the CCR unit. The operating temperature of the burner is 650 °C and a fuel named RFG is burned in the burners at 4.5 bar(g).

Soot is mostly formed in the vicinity of and agglomerated within the burner tip piece which is marked in the technical drawing below (Figure 3.1). Samples are obtained during the maintenance and cleanup of the burners. The RFG soot specimen was gathered by inserting a wire into the nozzle and letting remnants drop from the other side of the nozzle, in chunks, into a screwed test tube. It is then kept in a sterile bag under dark and dry environment. Samples are brought to the Clean Combustion Technology Laboratory of Mechanical Engineering Department at Middle East Technical University.

The samples used in these experiments are first gathered from burners that are shut down for the maintenance process.

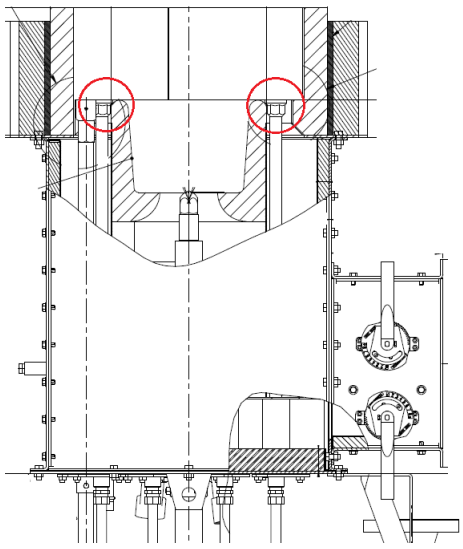

Figure 3.1 Burner tips marked on a sample burner design

Figure 3.2 Renewed burner tips

3.3. Soot Sample Preparation for Analysis

In this study, soot sample obtained from fuel gas nozzles were characterized. The soot sample from RFG combustion is named as FG in this study.

Soot samples are gathered from the clogged burner tips from a burner located in CCR unit in TUPRAS Kırıkkale Oil Refinery. Samples are obtained in one part, shaped as agglomerated chunks and processed afterwards in order to reduce the particle size.

The samples are first poured in a clean ceramic plate (Figure 3.3) and eye checked for impurities since the sample gathering environment is not controlled and in an open field. After the initial check, samples are put in a mortar and crushed and ground with a brass pestle (Figure 3.4). The reason of using mortar rather than ring mill or roll crushers is the limited amount of sample. The processed samples are then poured into series of sieves sized <106 μm and <75 μm. This step is done to eliminate any possible effects of size variance on the results and making the experiments more controlled in terms of physical size of the particles. The sieved samples sizing in 75-106 μm are collected and put in tubes.

Figure 3.3 Fuel gas soot (FG) sample gathered from the burner tips

Figure 3.4 Grinding in mortar

In the Continuous Catalytic Reforming (CCR) unit, naphthas which are treated with hydrogen are used in the reaction with the help of a catalyst called reforming catalyst. The products of the reactions are high-octane rated reformates, high hydrogen rated gases (net gas) and liquefied petroleum gas (LPG). Process schemes are provided in Figure 3.5 and Figure 3.6.

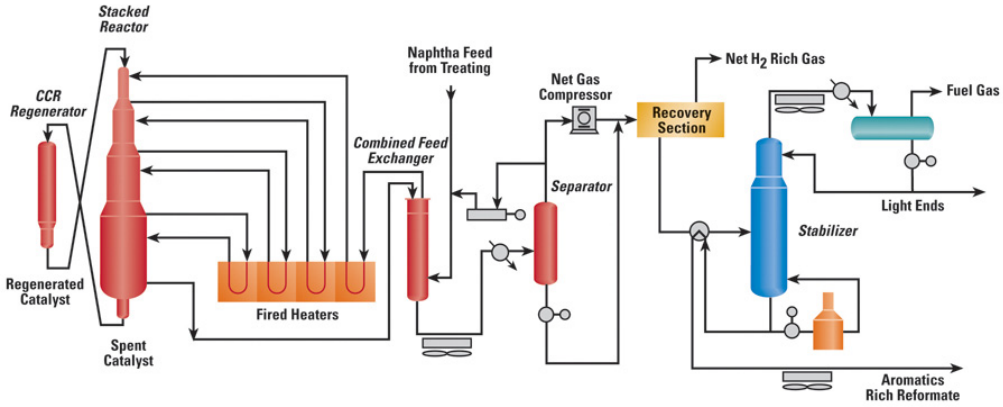

Figure 3.5 Process scheme taken from Honeywell UOP [64]

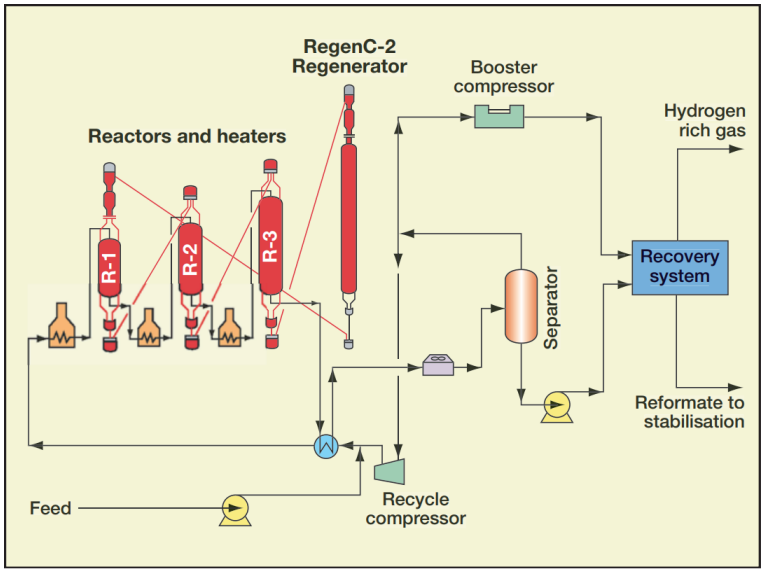

Figure 3.6 Axens CCR reforming process [65]

Both proximate and ultimate analyses of the soot gathered from the burner tips are conducted in various labs in Middle East Technical University (METU). Proximate analyses are carried out by a Thermogravimetric Analyzer (TGA) in Aerospace Engineering Department and the ultimate analyses are done by X-ray Diffraction (XRD) in the Thermal Analysis Laboratory, RAMAN in Infrared and Raman Spectroscopy Laboratory, High Resolution Transmission Electron Spectroscopy in Transmission Electron Microscopy (HRTEM) of the Central Laboratory of METU and Scanning Electron Microscope with Energy Dispersive X-ray (SEM-EDX) in the Electron Microscopy Laboratory of GÜNAM at METU.

3.4. Experiments for Soot Sample Characterization

The focus of this study is to determine the reactivity of the sample in order to determine at what (minimum) temperatures the gathered sample can be burnt and for this effect various analysis devices and methods are used.

Thermogravimetric analysis (TGA) and differential thermogravimetry (DTG) are preferred to obtain the data for the characterization of the sample. Since the gathered sample is an unknown material, XRD and RAMAN technique used to index the contents. FTIR is combined with TGA to have a detailed observation of TGA phases and to analyze what kind of gasses coming out of combustion taking place in TGA. For the morphological characterization, SEM and HRTEM are used.

3.4.1. Experimental Setup

Thermogravimetric analyzer

Thermogravimetry is a very common technique used in the literature to characterize the combustion or pyrolysis of the solid fuels. It is widely used because of being a simple and fast method.

In TGA, variation of mass of a solid sample is measured versus temperature change over time. The parameters having effect on TGA are; gas type, gas flow rate, temperature change rate. By recording the mass loss versus temperature, the phase transitions, thermal stability, oxidation and many other characteristics of a sample could be obtained. DTG (derivative thermogravimetry) is the derivative of the TG function expressing the reaction rate.

Fourier transform infrared analyzer

Another way of determining the reaction phases is analyzing the right side of the reaction, the outcoming gases. To do that, a device that collects data over a wide range of spectrum, which the infrared spectrum of absorption of a material, is needed. This technique is called Fourier-transform infrared spectroscopy (FTIR). In this thesis, FTIR device is coupled with the isothermal TGA experiments and as the TGA experiment continues, the exhaust gasses from the combustion is directed to the FTIR device. FTIR also helps determining what kind of elements/molecules exist in the sample.

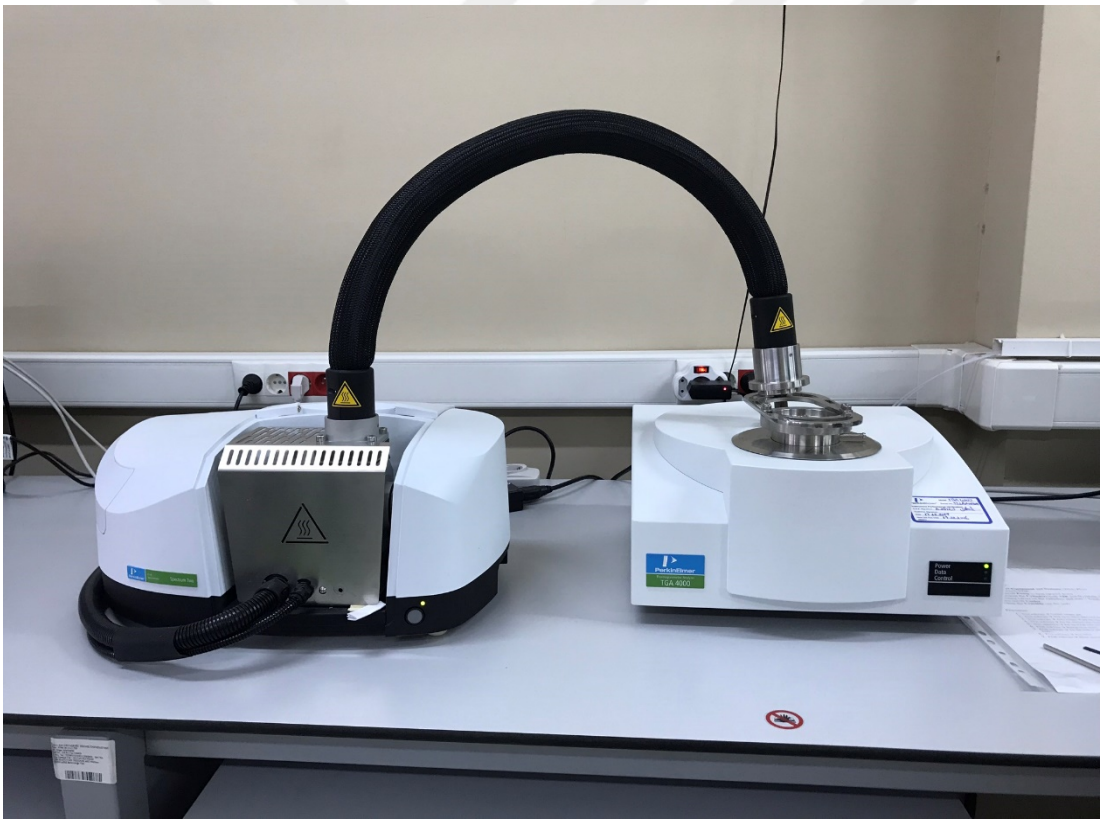

Figure 3.7. TGA and FTIR setup

X-ray diffraction

XRD is mostly used for identifying unknown materials. It provides the crystallographic density in other words crystal structure (characteristics) of crystalline materials as well as the quantitative analysis of phase composition, crystallite size and macro strain and texture orientation [66]. XRD allows determining the elements present in an unknown sample, their structure and material of it by shooting X-ray to it and monitoring diffracted waves from the sample. The diffracted waves have a wave pattern specific to the material itself. Because of the individual X-ray's being penetrated to the internal planes of a crystalline material reflecting from various layers of planes, there are a lot of waves interfering each other. This situation does not cause an issue for XRD since only the peaks of these interfered waves will be needed for XRD to extract data from a sample. The overlapped waves create "Constructive Interference" and "Destructive Interference" which helps us determine whether the recorded data is usable or not. "Constructive Interference" of waves form the peaks and these peaks will be compared with the database of material-XRD data library. Identifying the sample is done by cross checking the obtained data with the library.

Scanning electron microscopy

SEM scans an area by a focused electron beam. It images solid conductive samples under vacuum. The electrons interact with the sample and scatter regarding the density of the interaction and generates high resolution images. Unlike light microscopes that have x1500 magnification, SEM can reach a magnification amount of x100000, allowing researchers to observe micro and nano scale characteristics of solids. With SEM, morphology of the specimen, including surface topography and crystalline structure can be observed. In SEM, a specific set of coils are used to scan the beam in a raster-like pattern, and the electrons which are reflected of knocked off the near-surface region of a sample are detected (Figure 3.8). The interaction of electrons with the specimen generates backscattered electrons (BSE), secondary electrons (SE) and

X-rays. BSE and SE are primarily used for SEM imaging and these reflections transmit different information to the detectors. For instance, BSE images are very sensitive to differences in atomic number. Atoms with higher atomic numbers appear brighter in BSE images. Nonetheless, SE imaging provides detailed information about surface topology. When SEM is combined with another detector named EDX, X-rays can also be evaluated in order to detect what elements are contained in the sample.

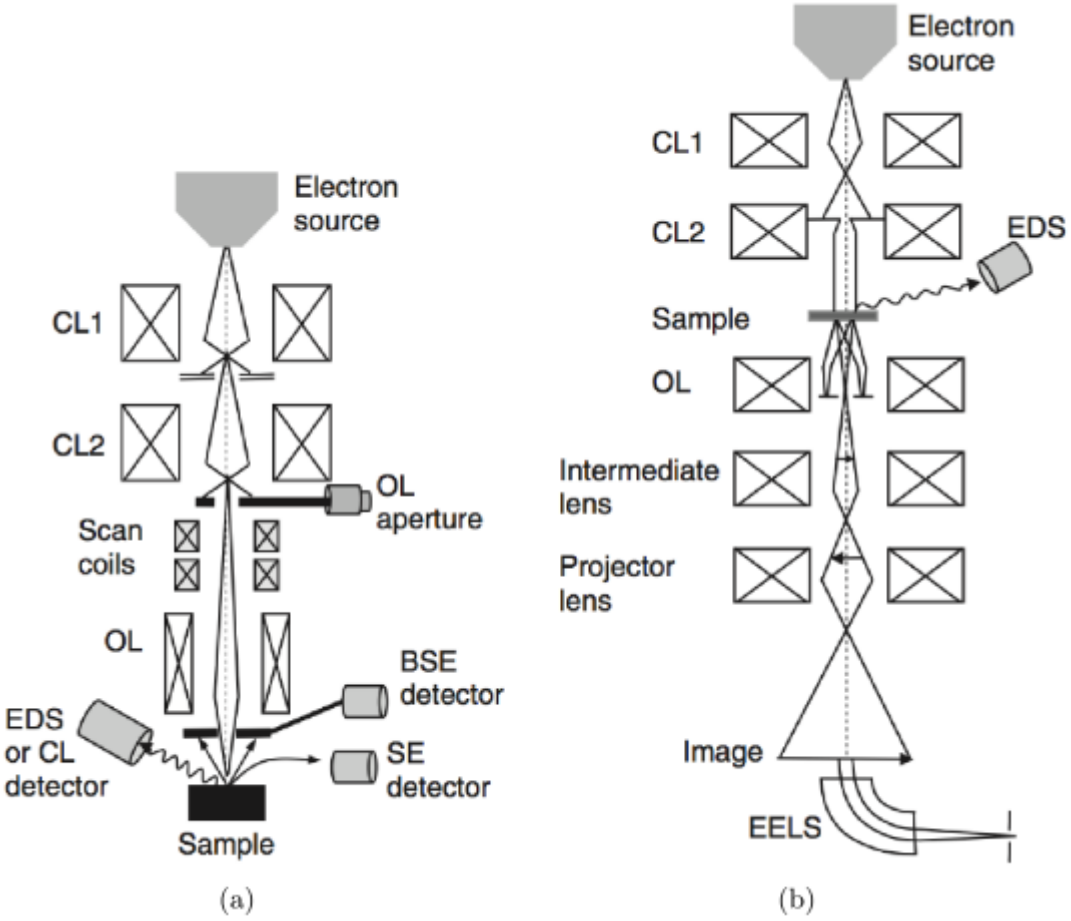

Figure 3.8 SEM Visual [67]

In this study, SEM and EDX analysis are done at GÜNAM at METU. Zeiss EVO HD15 is used to obtain SEM images and EDX scans.

Wire mesh reactor

A wire mesh reactor shown in Figure 3.9 is used to observe the reactivity of the fuel gas soot (FG) sample under high heating rates (~1600 ºC/s). The pyrolysis experiments are conducted using the setup at Clean Combustion Technologies Laboratory at Department of Mechanical Engineering at METU. For more detailed information on this setup the reader is advised to consult reference [68].

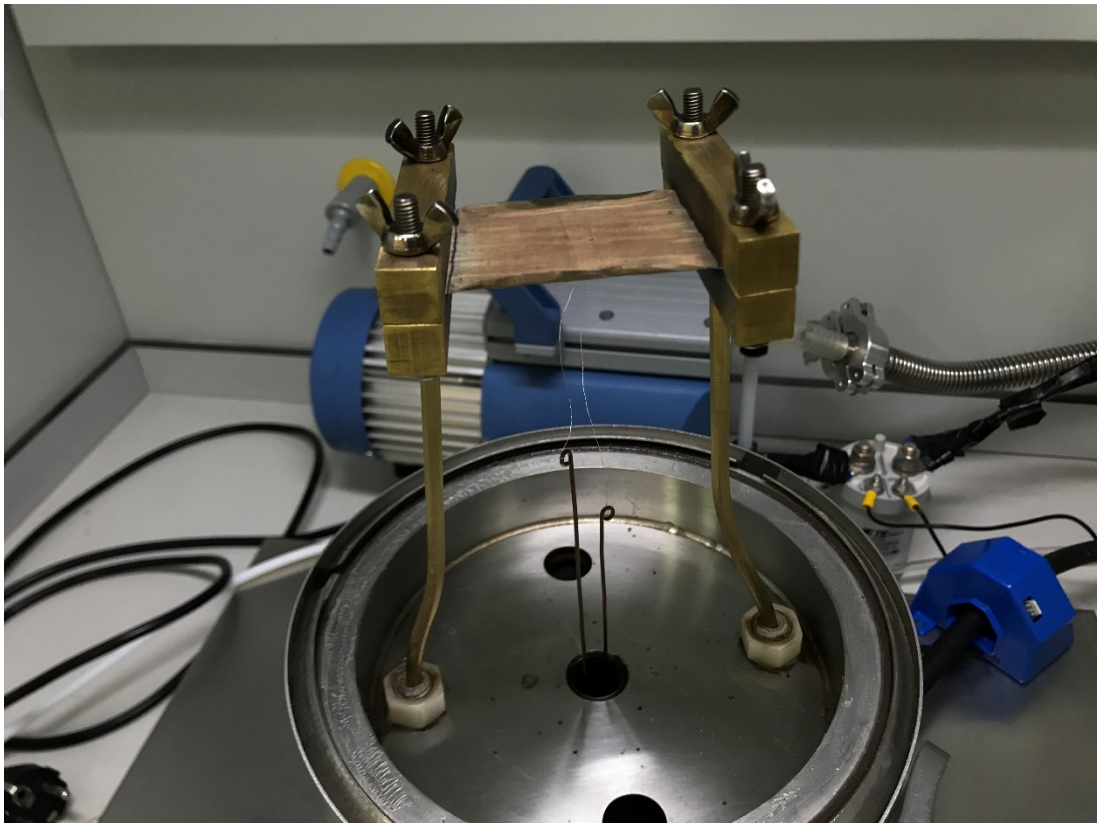

Figure 3.9. Wire mesh reactor setup

RAMAN

RAMAN spectroscopy is used for identifying molecules in a specimen. A monochromatic laser light is used to determine vibrational modes of molecules allowing researchers to identify the contents from its structural fingerprint. The laser photons' energy levels are shifted up or down regarding the interactions with other photons, molecular vibrations and other excitations from the system. The result is compared with the known shift patters from a library and corresponding molecules are reported. In this study, Renishaw/In Via dispersive RAMAN system is used at Central Lab at METU.

High-resolution transmission electron microscopy

TEM is a technique which uses the image of interaction of electrons as they are transmitted from an ultrathin layer of a solid or a suspension on a grid. The resulting image is magnified and focused on an imaging device and captured by it. In addition, HRTEM uses both transmitted and diffracted beams to create an interference image. This phase contrast image can be very detailed, as small as a single atomic column. In this study, JEOL JEM 2100F HRTEM microscope is used at Central Lab at METU.

3.4.2. Experimental Method

Thermogravimetric analyses are executed in Aerospace Engineering Department of METU. A Perkin Elmers TGA 4000 is used for the experiments. There are several conditions to be tested. The first step is to determine at what temperature the sample is combusted and to this effect a non-isothermal constant heating rate is chosen. Considering the applicability of the determined temperature value to the real case, for instance, if the burner tip can be able to be heated up to that value, the lowest possible value should be chosen in order not to deform the tip structurally during heating. The second set of experiments is done isothermally and to determine the behavior under minimum reactive temperature, that is obtained from non-isothermal TGA. The experiments are conducted twice in order to observe the repeatability.

There are four definable parameters during TGA experiments: temperature range, heating rate, gas composition and gas flow rate. Herein, for the non-isothermal experiments the samples are heated from 30 to 1000 ºC at 15 ºC/min under dry air with the flow rate of 100 mL/min. Slow heating rates are preferred in order to avoid significant limitations. After finding the lowest reactive temperatures from the non-isothermal experiments, the isothermal temperature(s) are chosen accordingly. For the isothermal experiments, the samples are initially heated to the desired temperature under nitrogen flow (100 mL/min), and the atmosphere is switched to dry air (100 mL/min) upon reaching the desired temperature. The determined isothermal temperature is 700 ºC.

The characteristic TG and DTG profiles are plotted as a function of the sample temperature. DTG plots are given to identify the stages of the combustion. The characteristic temperatures are determined and shown in Figure 3.10. The decomposition temperature where volatiles begins leaving the specimen is named as (T_v) which means that the weight loss is reached to 1 %/min after moisture release stage [54]. Then ignition temperature was determined by using TG-DTG tangent

method [52], [53], [69]. This is a graphical method that uses tangent, vertical, and horizontal lines and their intersections in order to determine the ignition temperature. These lines are illustrated in Figure 3.10. In this figure, first drawn vertical line (i) marks the peak combustion rate temperature (T_p) determined from the peak point of DTG plot. The tangent to the TG curve labeled as (ii) drawn from the intersection point of line (i) and the TG profile. The line (iii) represents the tangent of the plateau after the moisture release peak. Finally, line (iv) is drawn from the intersection of lines (iii) and (iv) vertically to determine the ignition temperature (T_i). T_e represents the end temperature when the sample burns out. It corresponds to the point where less than 1 %/min weight loss is reached [54].

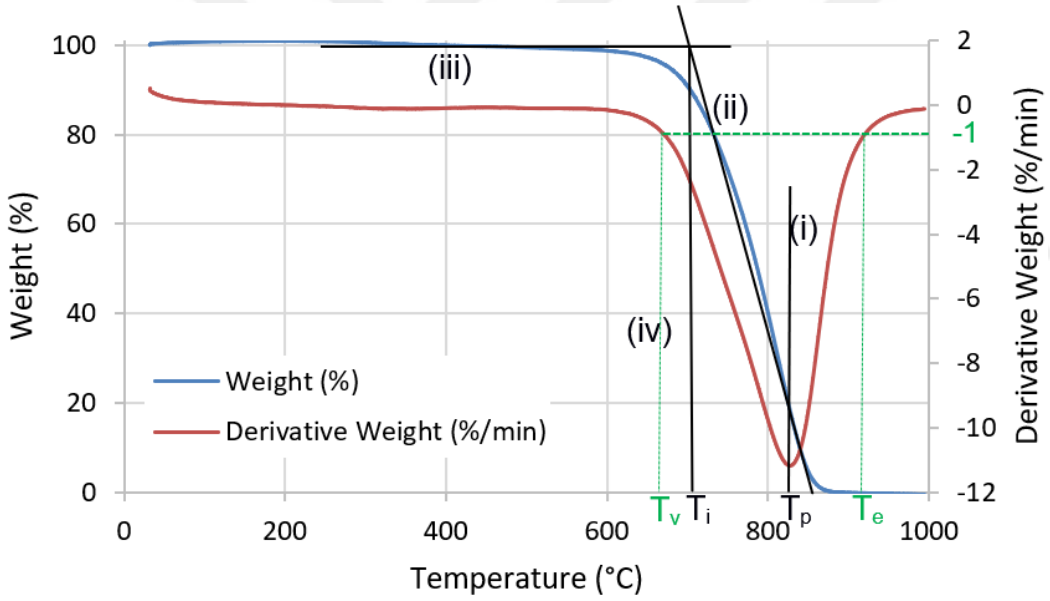

Figure 3.10 Characteristic temperatures during non-isothermal TGA experiments (T_v – decomposition temperature; T_i – ignition temperature; T_p – peak temperature; T_e – end temperature)

During isothermal experiments, the TGA is coupled to an FTIR apparatus. These experiments are also done by having dry air as the gas, with the flow rate of 100 ml/min. FTIR has a heated hose kept at 270 ºC to avoid condensation of the gasses

passing through. The Perkin Elmer Spectrum Two FTIR device has a capability of measuring a wavelength range of 8300-350 cm^{-1} with a maximum resolution of 0.5 cm^{-1}. The experiments in this thesis are done in the range of 4000-450 cm^{-1} with resolution of 1 cm^{-1}.

FTIR analysis is based on a law found by Johann Heinrich Lambert and August Beer. Beer-Lambert law dictates the relationship between the absorption of light and the material properties that is travelling through [70]. This law proposes that there is a linear relationship between the gaseous mediums and the spectral absorbance at a specific wavenumber. In Figure 3.11 the transmittance of the most relevant gas molecules formed during combustion of the sample is presented.

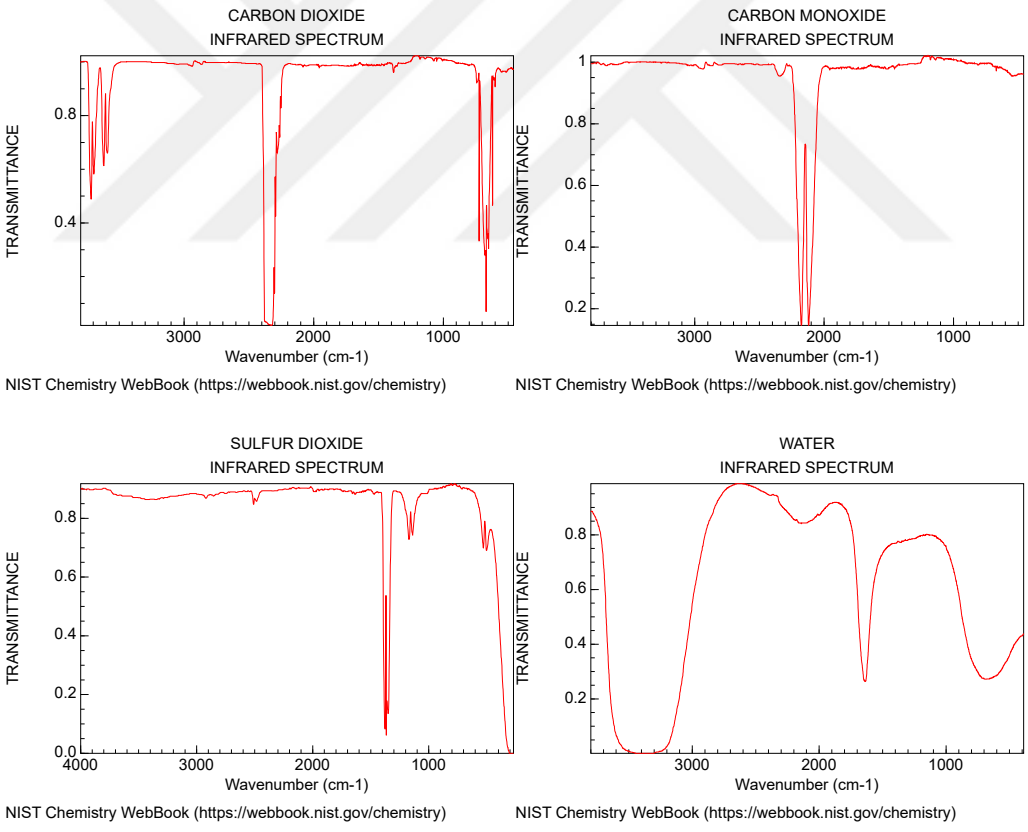

Figure 3.11 IR Spectrum of CO_2, CO, SO_2 and H_2O

Regarding the graphs, ranges of where the transmittance value gets close to zero will be evaluated and considered positive existence of the related gas molecules. In this thesis, CO_2, CO, SO_x and H_2O molecules are investigated.

Further experiments are done in order to gather morphological information.

Scanning Electron Microscopy (SEM) was used to observe the particle shape and morphology of the fuel gas soot (FG) sample. Non-coated FG soot sample is placed on a carbon tape and analyzed under low vacuum condition. Analysis was performed using a Zeiss EVO HD15 instrument, with magnifications between ×100 and ×5000.

Crystalline structure data is analyzed from X-ray diffraction. XRD experiments are conducted for FG sample in METU Central Laboratory in a Rigaku Ultima-IV instrument. The scan range of XRD is 3 to 90º, scan speed is set as 1 º/min and the sampling width is 0.02º. Given below are the XRD measurement conditions.

Table 3.2 XRD measurement conditions

XG	Cu/40 kV/30 mA
Duration time / Scan speed	1 deg/min
Step / Sampling step	0.02 deg
Measurement axis	2theta/theta
Scan range	3-90 deg

3.4.3. Measurement Errors and Uncertainties of Experimental Methods

In every experimental analysis, there are some measurement errors and uncertainties of random amounts because of the possible inaccuracies in measurement equipment.

For TGA, values of weight and temperature may change depending on the measurement errors at the time of the experiments. FTIR spectrometer also has some

measurement errors yielding some uncertainties in the results. TGA analyzer have ±1 ºC temperature accuracy with ±0.8 ºC temperature precision and ±0.02% balance accuracy with ±0.01% balance precision. The FTIR device has the wavelength accuracy of 0.1 cm-1 at 1600 cm-1.

SEM-EDX, TEM, XRD and RAMAN may have some measurement errors because of the uncertainties of the sensor data. Technical specifications from these devices can be found from the manufacturer's website.

CHAPTER 4

RESULTS AND DISCUSSION

In this section of the thesis, experimental results are expressed and discussed. As the main purpose of this thesis is getting to know about the soot remnants on the burner tips and putting forward a solution to eliminate it, outcome of the experiments is also discussed considering industrial applicability.

Thermogravimetric (TG) and derivative thermogravimetric (DTG) results are used primarily to determine the ignition temperatures (T_i). TGA experiments were conducted in non-isothermal (Figure 4.2) and isothermal (Figure 4.3) conditions. Non-isothermal TGA designates T_i at which isothermal experiments were conducted. Target temperature used in isothermal TGA is the lowest sustainable combustion temperature of the fuel gas soot (FG) specimen.

At the early stages of this study, the sample contents were not entirely known. To identify the composition of the FG specimen, FTIR of exhaust gasses of TGA are analyzed in Figure 4.4 and . Although the precursor (RFG) of FG specimen contains hydrogen and sulfur, FTIR gave no traces of both. Hence further unknown material identification methods, such as EDX (Table 4.2), XRD (Figure 4.14 and Figure 4.15) and RAMAN (Figure 4.16) are used. Combustion phases and their meanings are also indicated under subsection 4.1.

Since the SEM images are not sufficient for identification of soot particles, in addition to that, HRTEM technique (Figure 4.12) is used.

Combining these methods and techniques, this section is presented under three subsections: Thermogravimetric analysis, WMR Analysis and Morphology, Chemical Composition and Structure.

4.1. Thermogravimetric Analysis of Soot Sample Derived from RFG Combustion

In this section, characteristic temperatures of the TG and DTG experimental data (Figure 4.2 and Figure 4.3). Exhaust gasses are measured with FTIR during TGA's of FG specimen and provided together with corresponding DTG curve (Figure 4.4 and Figure 4.5). Effect of high heating rates are also discussed in section 4.2.

RFG used in burners contains almost no inorganics (main fuel's composition is given in section 3.1). Expectation is that, soot formation from combustion could consist of some inorganics because of the impurities and corrosion coming from the pipelines. However, as it can be seen from Figure 4.2 and Figure 4.3, FG sample burns completely and there is no remnants such as inorganics or ash left on the crucible of TGA.

Some characteristic temperatures are named as follows: T_v: temperature where the volatiles start vaporizing, T_i: temperature of the initiation of the combustion, T_p: temperature where the maximum combustion reaction speed is reached, T_e: temperature where the combustion finishes.

In the non-isothermal experiment, where the sample is heated up to the 1000 °C at 15 °C/min heating rate, the behavior of the FG soot sample is observed, which can be seen in Figure 4.2. 5 mg from the 75-106 μm particle sized FG sample is used for this experiment. TGA data can be divided into sections in order to further understand the behavior of sample during these stages (see Figure 4.1). The first phase starts from t=0 s. As the temperature reaches 100 °C, moisture is completely removed, and some other volatiles begin evaporating and leaving the TGA furnace. The second section starts with the initiation of combustion (T_i). T_i propounds the lowest temperature that should be reached in order to eliminate the soot from the burner tip. Therefore, it is an important data point for this study. T_m is the peak point of the DTG graph. It is the

temperature which the fastest combustion reaction speed is reached. Last characteristic point, T_e, is the temperature where the combustion reaction finishes. T_e can change depending on the heating rate.

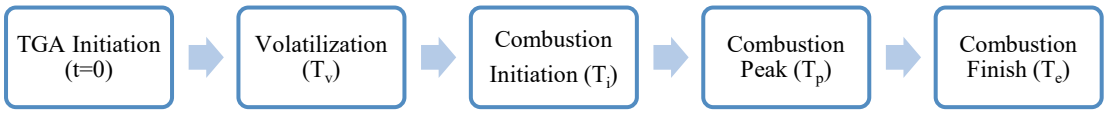

Figure 4.1 Characteristic combustion temperatures for non-isothermal TGA

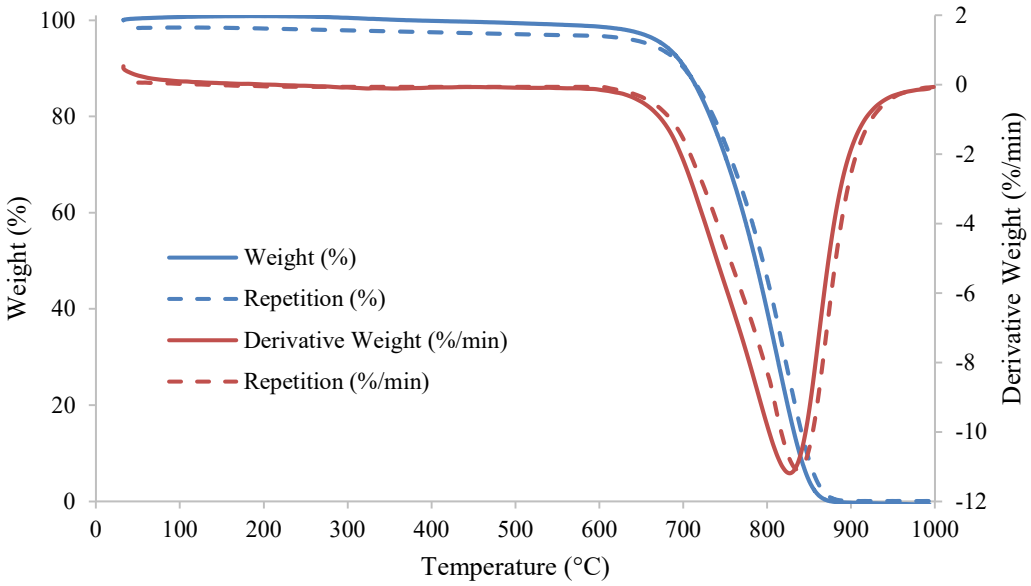

Figure 4.2 TG and DTG profiles for the non-isothermal combustion of the fuel gas (FG) soot sample at a heating rate of 15 ºC/min (5 mg, 75-106 µm particle size)

The second kind of experiments are conducted under isothermal conditions (see Figure 4.3). When the specified temperature was reached, TGA chamber gas is switched to dry air and temperature is kept constant until the end of the analysis. This specific temperature is named as, target temperature (T_t) in this thesis. Until the target

temperature is reached, TGA furnace is kept under an inert gas (nitrogen), which inhibits any oxidation reaction. In isothermal TGA, since the analysis begins with an inert gas, the phase between (T_0-T_t) allows researchers to observe the weight change effect of demoisturization.

Following is the characteristic temperatures of the non-isothermal experiments. Temperature where volatiles start leaving the sample (T_v) is ~630-640 °C and the point where sample ignites (T_i) is ~700-720 °C. Fastest combustion (T_p) takes place at ~815-830 °C and combustion ends (T_e) at ~915-920 °C.

Non-isothermal analysis introduced general behavior of the FG sample between a temperature range of 30-1000 °C. It can be concluded that at any temperature higher than T_i=700 °C, the sample can be oxidized. In order to observe this in detail, second kind of TGA analyses are done, in which the temperature is increased under an inert gas (nitrogen) and air is injected after the pre-determined temperature is reached and kept constant throughout the analysis. After injected gas has changed to air, combustion starts immediately and completed in 15 minutes (Figure 4.3).

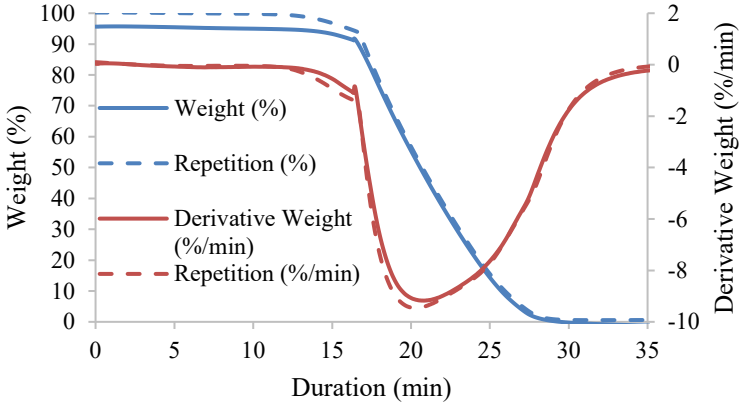

Figure 4.3 TG and DTG profiles for the isothermal combustion of the fuel gas soot (FG) sample at 700 ºC (5 mg, 75-106 µm particle size) (2 repetitions)

In the study of S. Lebedkin et al. [55], results of single walled carbon nano tubes (SWNT) are compared with graphite TGA given in this thesis. Considering lower heating rate he used, increased burnout temperature in this study could be due to the heating rate differences. This study also provides full burnout of the sample as in the study of S. Lebedkin et al [55].

In this study, FTIR analysis is done for the FG sample. FTIR shows the emission gasses of the combustion, therefore gives an idea about the sample composition. CO_2, CO, H_2O and SO_x molecules are sought since the fuel being burnt in the burners consist mostly of organic molecules and a very little amount of H_2S. In the results, traces of SO_x and H_2O cannot be found. FTIR data are provided with DTG curve and both data are pivoted around the gas injection point. The repetition experiments are given in Appendix A.

In Figure 4.4, FTIR data of CO_2 shows a rapid increase when air is injected to the TGA chamber. After air injection, purging nitrogen fully from the combustion chamber and spaces between particles takes 3-4 mins, air reaches to the maximum of the surface of the specimen and combustion rate reaches its maximum.

FTIR data of CO shows the rapid increase point is where the combustion starts (Figure 4.5). The CO existence, from air injection to the end of the experiment, is caused by insufficient contact of sample with air which is expected for solid fuels since air cannot penetrate among the lower particles of the sample. In addition, there could be a diffusion limit occurring during the experiment. The crucible has a cylindrical shape. If the crucible had a wide area that we can put the sample and spread it finely, CO generation will be much lower due to having more complete combustion on the surface and better air penetration to the lower parts of the sample stack.

If the sample consists of hydrogen, it can be observed by examining the wavelength range of H_2O (see Figure 3.11) in FTIR data. H_2O can be expected since it can be seen from Table 3.1, that there is a considerable amount of H_2 exist in the RFG. This is because vapor pressure of steam is higher compared with CO_2 and CO and it leaves

the furnace environment very fast that they were not adsorbed by the soot sample. As a result, no signs of H_2O are observed in FTIR results.

Another expectation is emission of SO_2 or SO_3 from TGA, that can be called as SO_x. It can be seen from Table 3.1, that there is a trace amount of H_2S exist in the RFG. It is well known that Sulphur is more reactive than Carbon atoms. Therefore, Sulphur leaves the furnace environment before Carbons. This is the possible reason of not observing Sulphur content in the soot sample. As a result, no signs of SO_x were observed in the range.

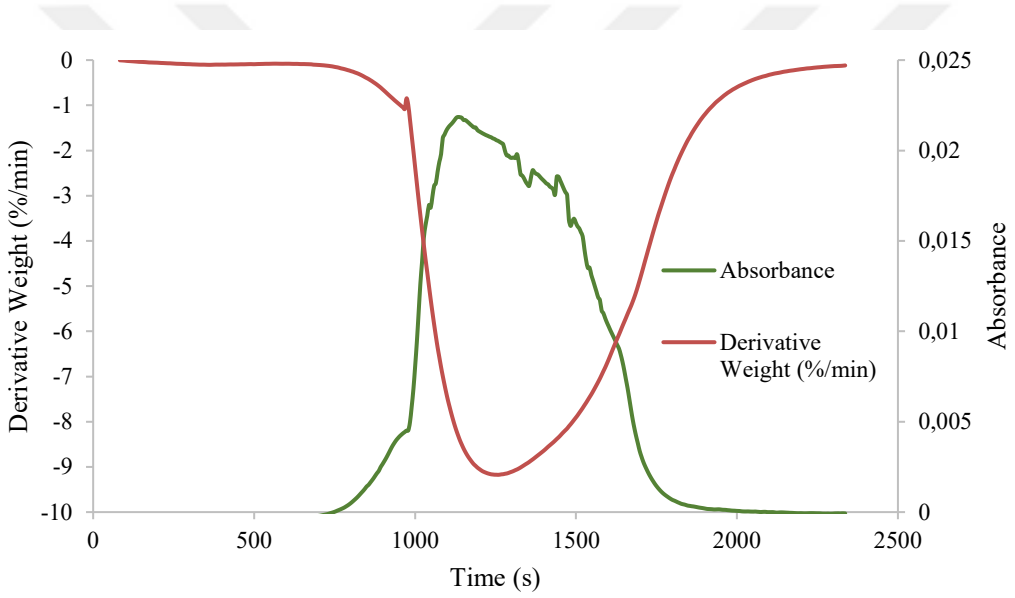

Figure 4.4 DTG profile and FTIR absorbance spectrum of CO_2 of the isothermal combustion of the 75-106 µm fuel gas soot (FG) sample at 700 ℃

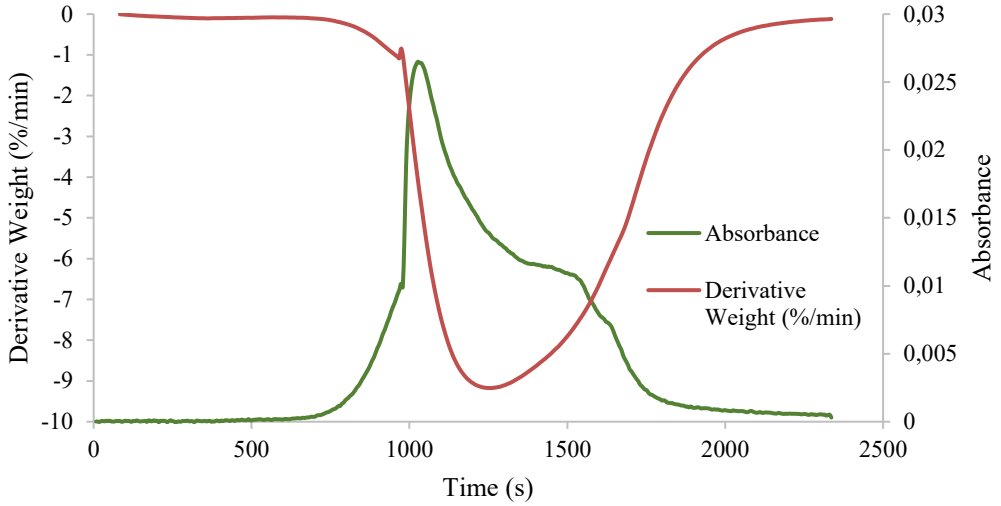

Figure 4.5 DTG profile and FTIR absorbance spectrum of CO of the isothermal combustion of the 75-106 µm fuel gas soot (FG) sample at 700 ºC

Regarding the results given, even after the unwitting soot formed in or around the fuel nozzles, if the burner tips are heated up to 700 °C and kept the temperature for 15 minutes, the soot remnants will burnout completely. In order to do that, passive heaters, such as electrical tracings, could be put around the burner tips that are capable of heating the tip up to 700 °C. Depending on the soot formation frequency around the burner tip, these electrical heaters can be triggered for the given duration and shut off after.

4.2. Wire Mesh Reactor Analysis of Soot Sample

In order to see the effect of heating rate, a wire mesh reactor that can reach heating rates of 1600 °C/s is used. High heating rates may change structure of carbons in the sample and cause different results.

Heating rates of 720 °C/s and 800 °C/s is preferred to imitate the average temperatures that the sample burns in TGA experiments. Samples are kept at desired temperature for 25 s in the reactor and resulting yield values are recorded. Yield values can be found in Table 4.1.

Sample behaves different when the heating rate increased. Under 15 °C/min heating rate in TGA experiments, FG specimen burned completely, while WMR (heating rate of 800 °C/s) results showed a ~4% yield. The specimen may be changing its structure because of the very high heating rate.

Table 4.1 Wire mesh experimental conditions and fuel gas soot (FG) sample yields

Temperature (°C)	Residence Time (s)	Sample (mg)	Yield (mg)	Yield (%)
720	25	4,9	0,2	4,08
800	25	5,1	0,2	4,76

4.3. Morphology, Chemical Composition and Structure of Soot Sample

In this section morphological features and composition of the sample are discussed using SEM-EDX, XRD, RAMAN and HRTEM techniques.

4.3.1. SEM and EDX Results

Two particle sizes are observed under SEM and their EDX results are given at the end of the section. EDX results explicitly show that almost all of the images are consisting of the same type of elements, which is carbon.

The FG soot sample was gathered from its natural formation zone and unlike laboratory generated particles, it was in agglomerated form when it was gathered. This can be clearly seen from the microscopic images. Particles are in agglomerated form and varying in shape and size. Figure 4.6 and Figure 4.7 represents that on the surface of the particles, chain like soot structures exist.

Because of the agglomerated structure of the FG specimen, soot particles could not be observed clearly under SEM. In order to observe soot particles properly, the need for TEM technique arised.

Some particle size measurements are also included in the images. Wider image is given in Appendix A.

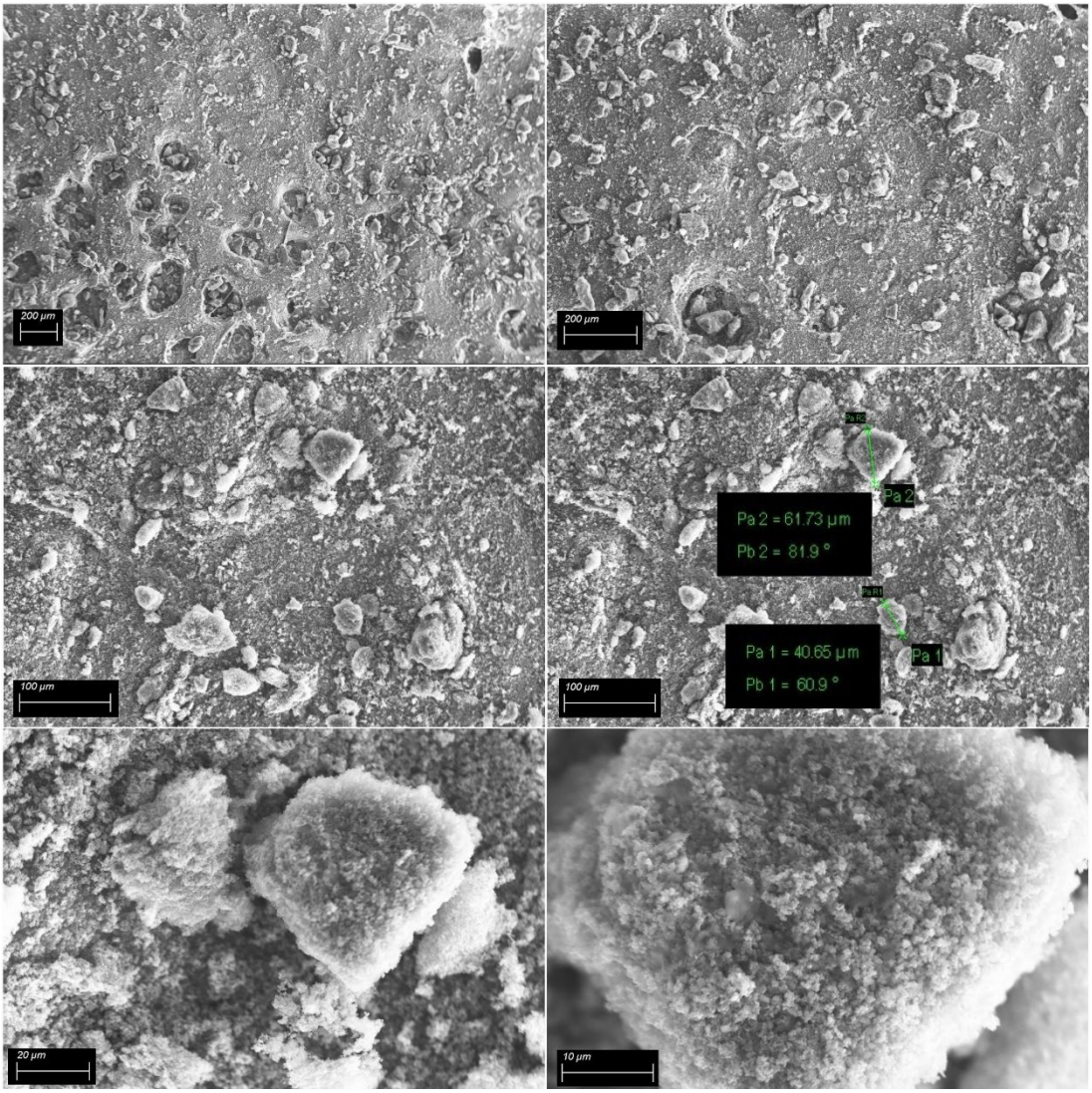

Figure 4.6 SEM images of 0-75 µm particle sized fuel gas soot (FG) sample

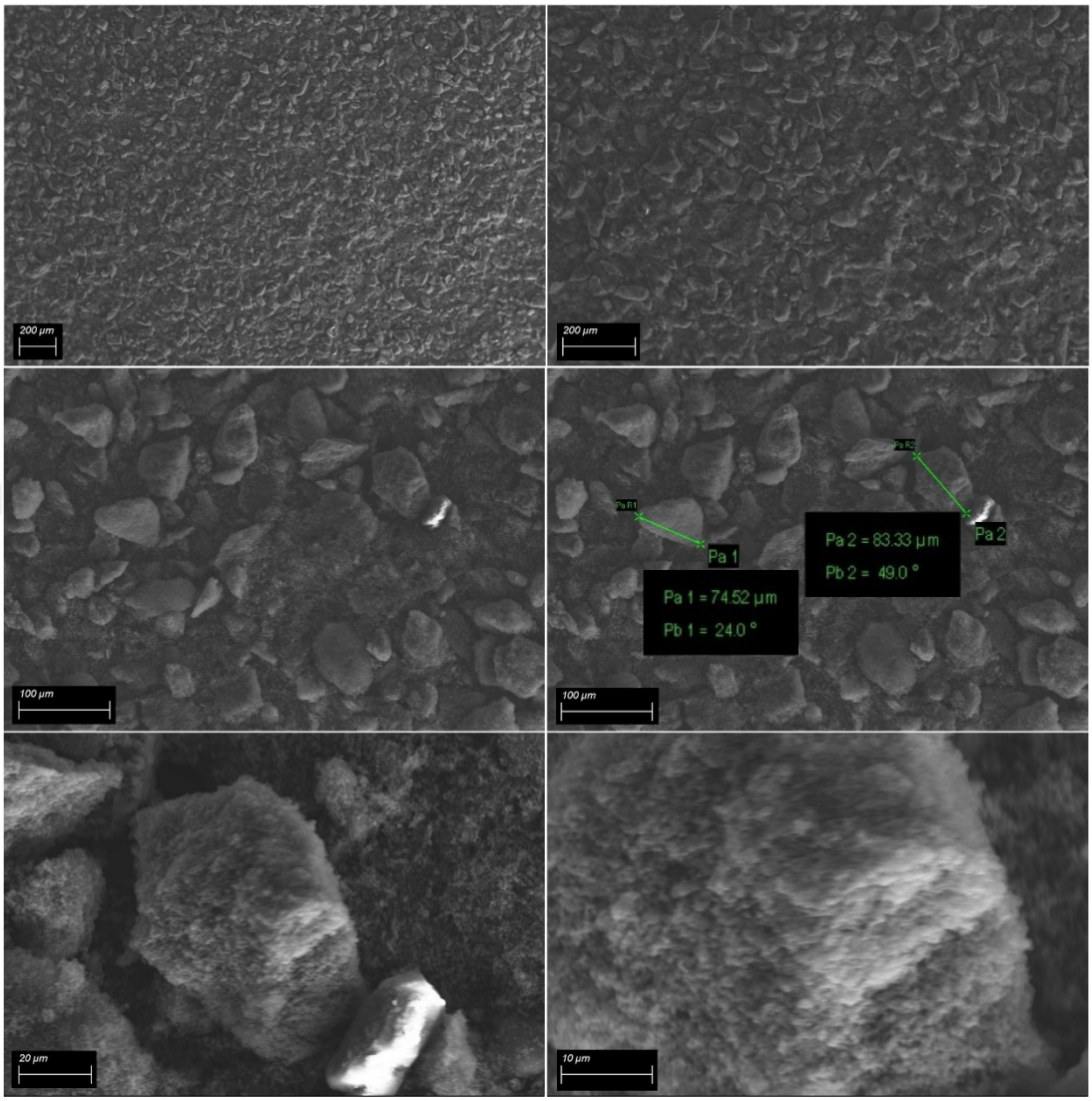

Figure 4.7 SEM images of a 75-106 µm particle size of fuel gas soot (FG) sample

SEM images from the studies of Dikio et al. [26] appear similar to the ones in this study. The pseudospherical and chainlike structure can be observed from both results.

4.3.1.1 EDX Results of SEM Images

In this section, EDX results are given in Table 4.2 and their evaluation area is marked on corresponding SEM images. While observing SEM images, a particle which has a different brightness is observed (see Figure 4.9). The elemental analysis of this particle is marked as the scan number 2 which can be found in Table 4.2. This is the only impurity found in the SEM images. Detailed results are given in Appendix A.

Table 4.2 EDX results of the sample images by scan number

Scan #	Element	Wt %	Atomic %	Error %
1	C	100.00	100.00	1.42
2	C	49.48	59.97	10.85
	O	35.05	31.89	12.58
	Al	5.76	3.11	8.14
	Si	9.71	5.03	6.37
3	C	100.00	100.00	1.27
4	C	100.00	100.00	1.33

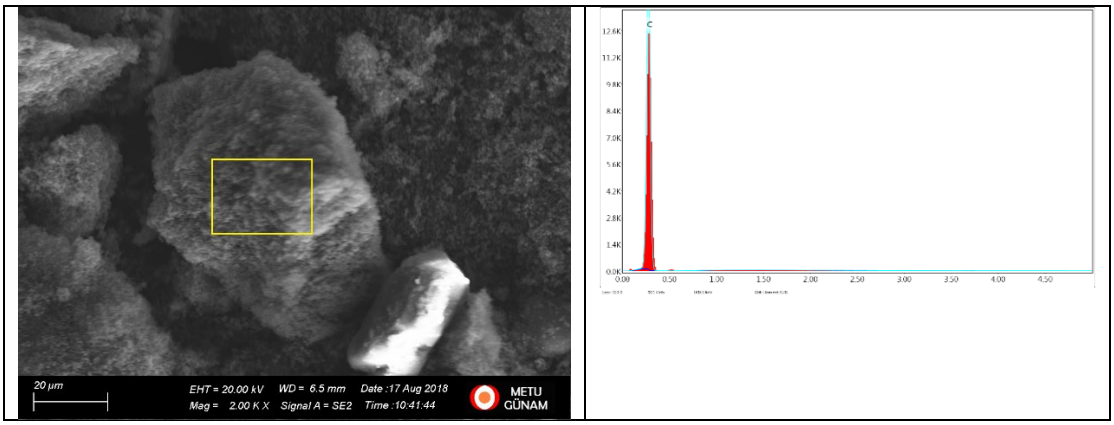

Figure 4.8 Selected area and results for EDX scans #1 for 75-106 µm particle sized fuel gas soot (FG) sample

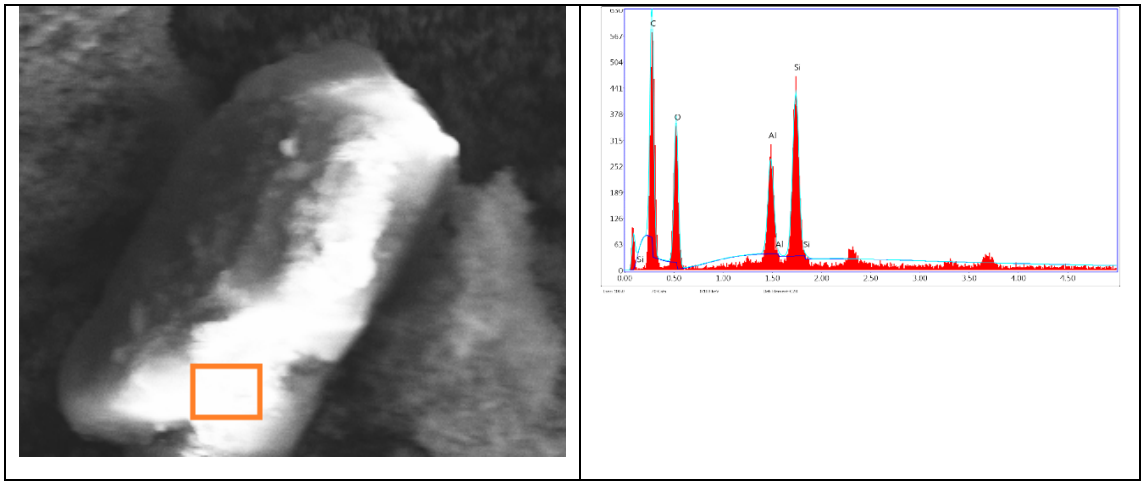

Figure 4.9 Selected area and results for EDX scan #2 for 75-106 µm particle sized fuel gas soot (FG) sample

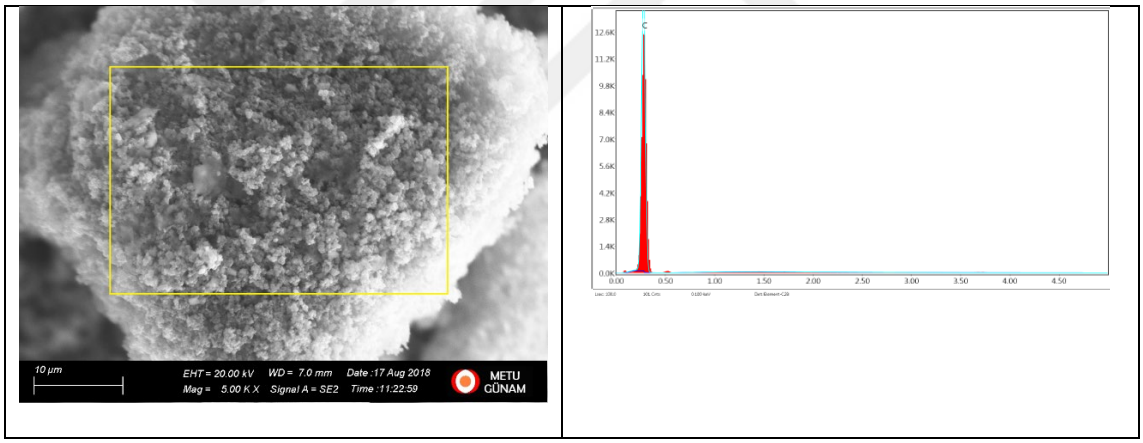

Figure 4.10 Selected area and results for EDX scan #3 for 75-106 µm particle sized fuel gas soot (FG) sample

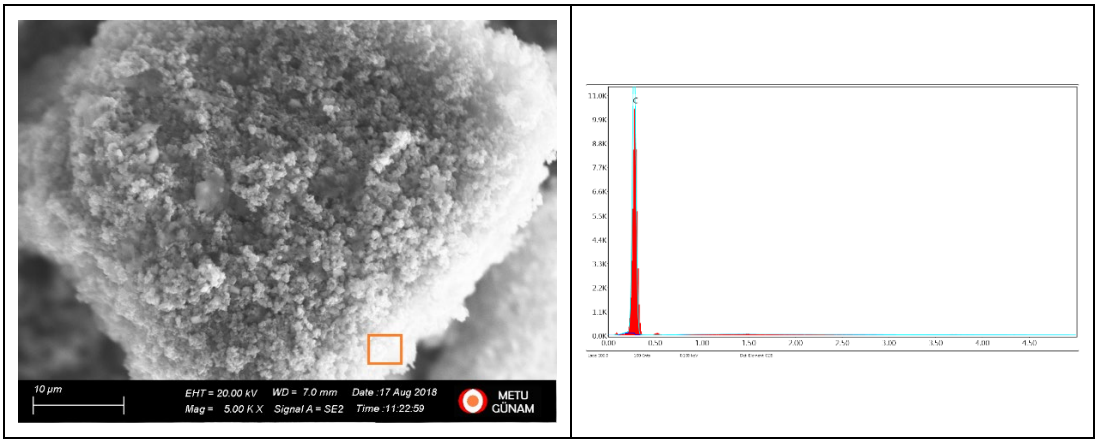

Figure 4.11 Selected area results for EDX scan #4 for 75-106 µm particle sized fuel gas soot (FG) sample

In terms of surface geometry, SEM pictograms correspond with the one in the study of Dikio et al. [26].

4.3.2. HRTEM Results

HRTEM micrograms show chain like structures of carbon. Close up images reveal the interatomic geometries. Structure of soot is crystalline in amorphous carbon matrix and it does not have any graphene planes, and it has some deviations of interatomic distances in the order of mesoscopic scale (≃1 nm). Wider image is given in Appendix A.

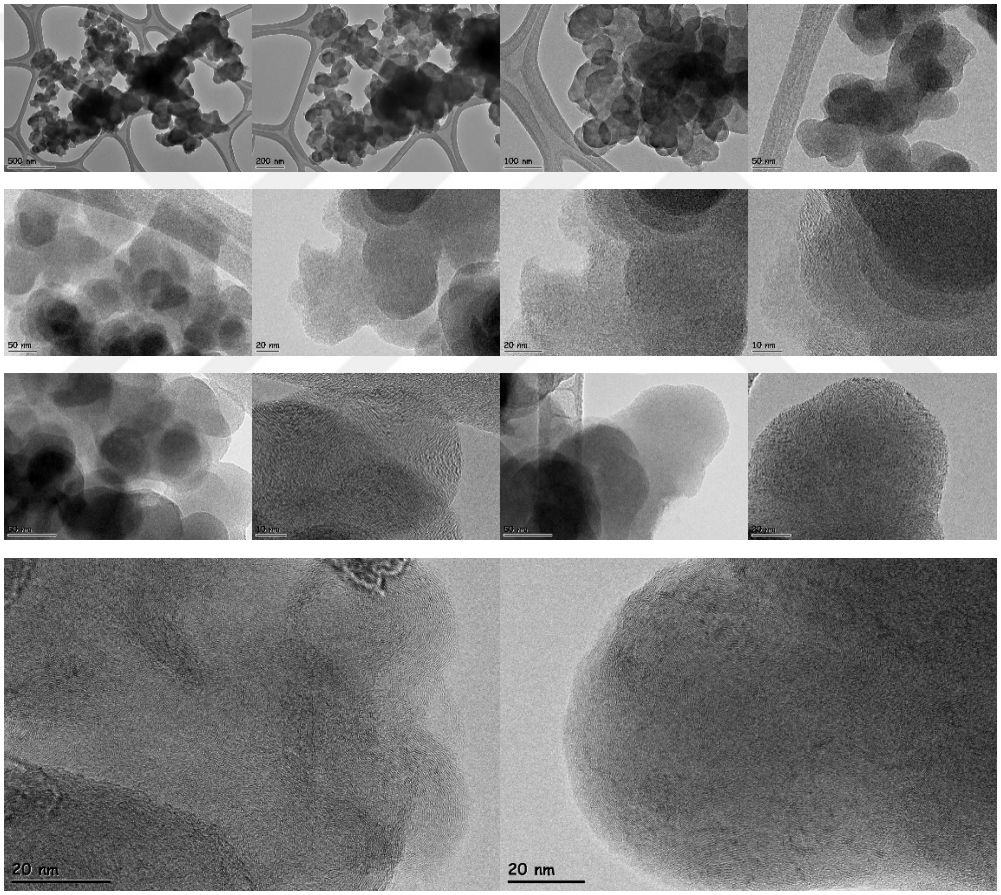

Figure 4.12. HRTEM micrograms of FG soot sample

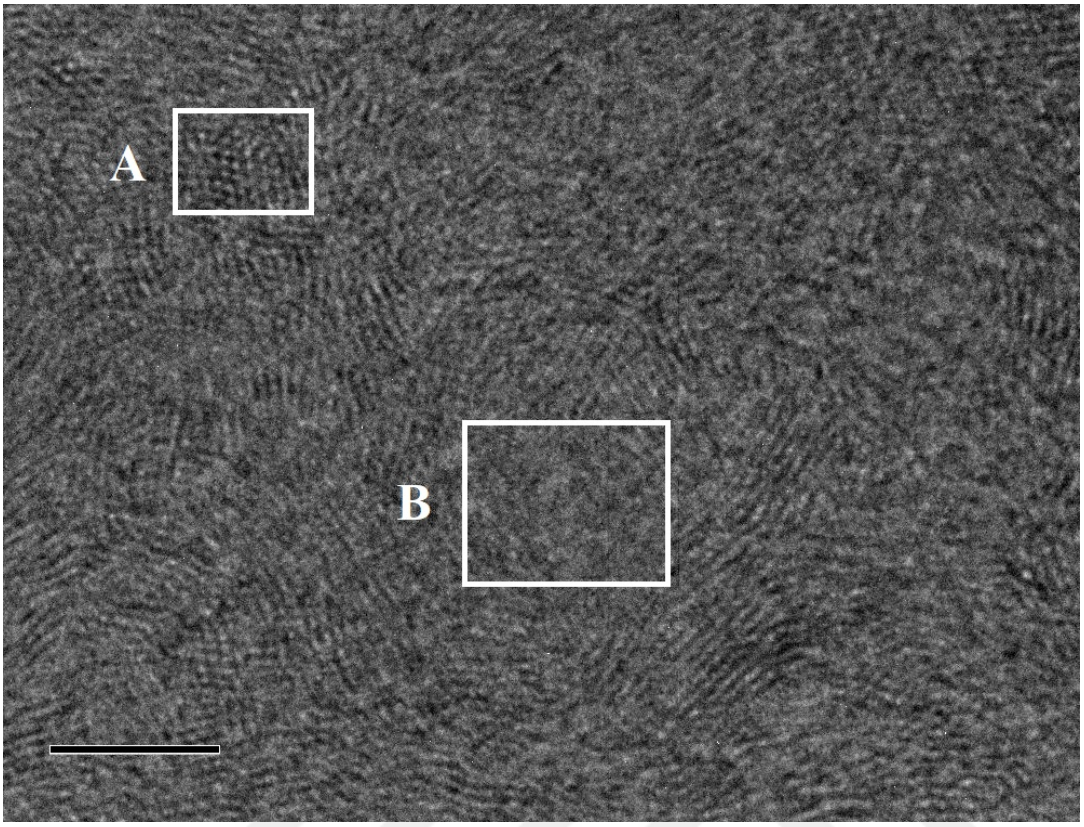

Figure 4.13. HRTEM micrograms of FG soot sample (A: indicates ordered region of carbon atoms, B: amorphous region) (solid line corresponds to 5 nm)

Micrograms corresponds with the ones in M. Alfè et al. [59], [60] who studied methane soot, Park et al. [61] who studied soot from ethanol droplets, and Castoldi et al. [62] who studied Printex U as a modal soot.

In comparison with A. M. Vargas et al. [63] soot samples subject to this study is in agglomerated form. Samples look a lot bigger than the ones in the study of A. M. Vargas et al [63].

4.3.3. XRD Results

SEM images prove that the sample is mostly uniform in terms of elements it consists of. XRD verified this and provide us additional information about carbons' crystalline structure. XRD results show that the sample consists of crystalline structure which is Graphite-2H.

Although XRD indicates a crystalline form of carbon, TEM shows that even though it has crystalline structure at some nodes, most of the carbons in the specimen are in amorphous form. XRD can only show peaks of crystalline structures since the X-ray diffraction occurs only on these kinds of substances. The broad first peak implies that there are large amounts of amorphous material exist in the sample. Width of the second peak being broad also implies that there may be some other low-quality forms of carbon exist in the FG sample. Pure graphite XRD's have narrower peaks compared with the one in this study. Amorphous materials do not show any peaks or broaden the existing ones when they are analyzed in XRD. Since the sample is a by-product of combustion, it is expected to have a heterogenous structure including both crystalline and amorphous carbon. Detailed results are given in Appendix A.

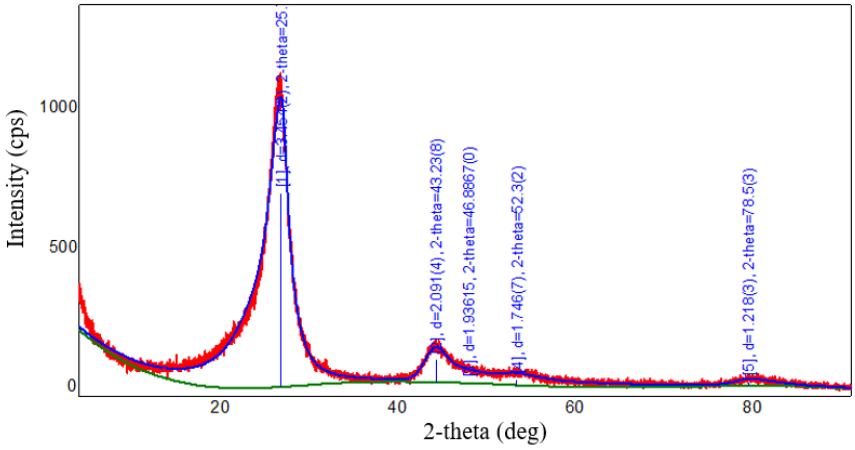

Figure 4.14 XRD raw data peak comparison with graphite-2H peaks

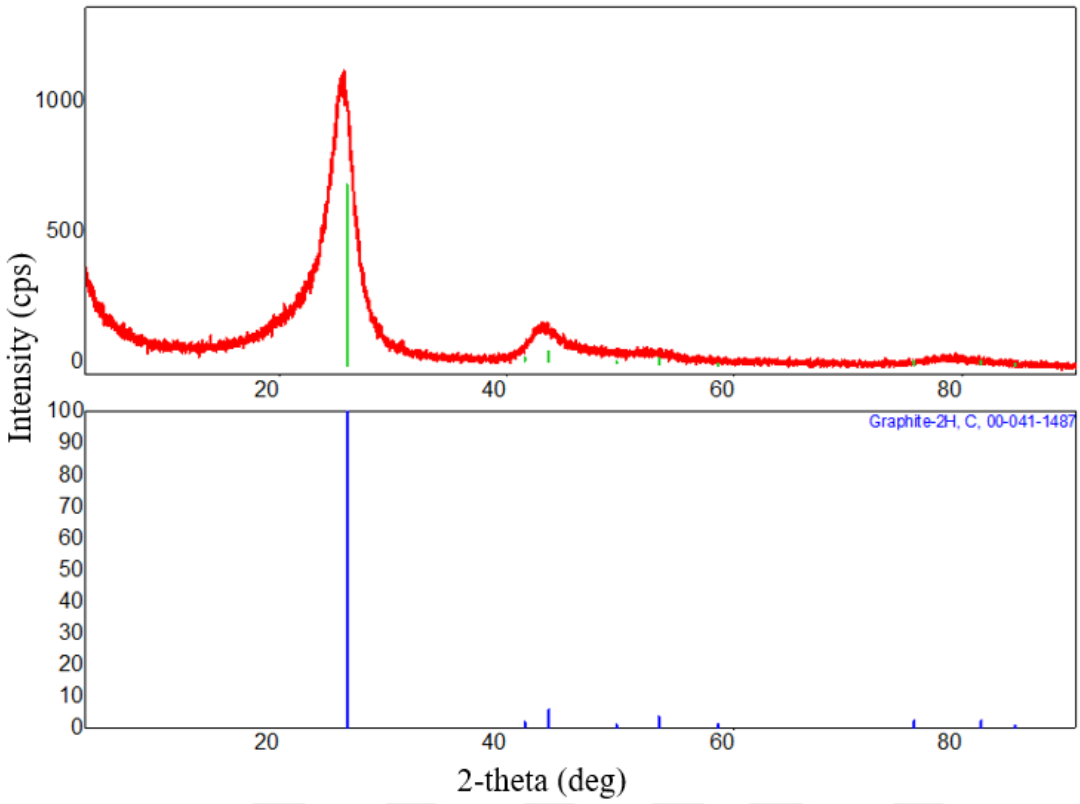

Figure 4.15 XRD data with graphite-2H peaks (simplified view)

These values also correspond with in the study of Dikio et al. [26] which has peaks at 23.68 and 42.33 2θ results.

4.3.4. RAMAN Results

To the further inspection of dominant carbon phase of the FG specimen, RAMAN spectrography is done which can be seen in Figure 4.16. RAMAN result shows a similar result with the one in TEM, that the dominant structure of the carbons in the sample are amorphous. The peaks around 1330 and 1583 shifts are common in the literature [26], [58].

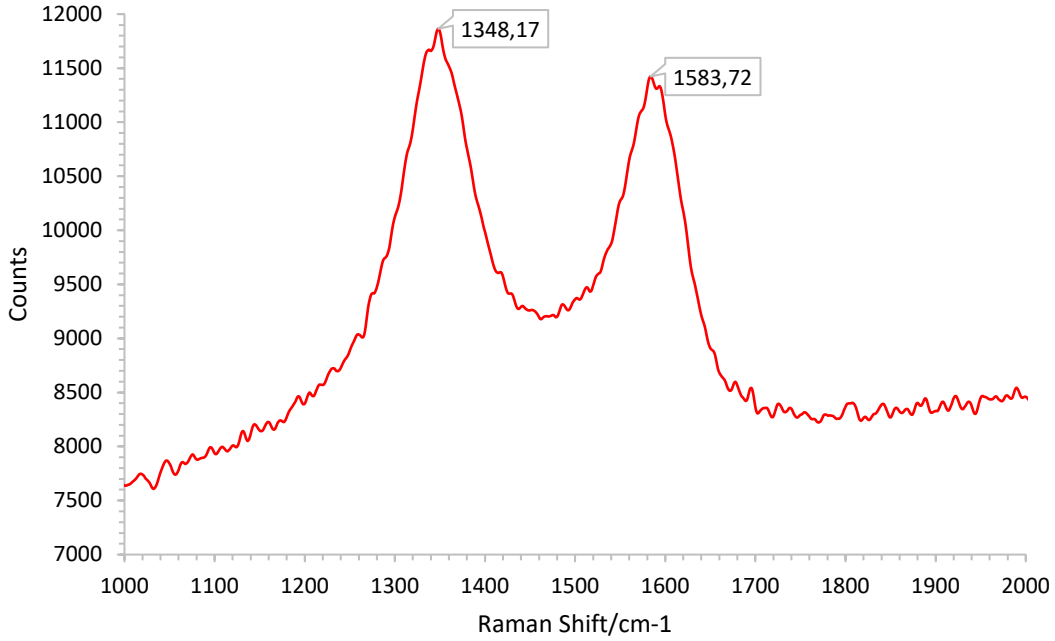

Figure 4.16 RAMAN of the fuel gas soot (FG) sample @532 nm laser edge

The found result corresponds with the studies in Dikio et al. [26] and Dychalska et al. [58].

CHAPTER 5

CONCLUSION AND FUTURE STUDY

5.1. Conclusion

In this thesis study, soot formation and its components are studied. To develop a better insight into its composition, TGA coupled with FTIR apparatus, WMR, SEM-EDX, HRTEM, XRD and RAMAN analysis and techniques are used.

As a result of TGA analysis, it can be concluded that the T_i for the sample is ~700-720 °C and in isothermal TGA at 700 °C, the full burnout is taken 15 minutes.

As an outcome of the WMR analysis, it can be concluded that higher heating rates of 720 °C/s and 800 °C/s affect the yield amount. Unlike TGA results which are shown 0% remnants, WMR results are shown 4-5% of yield. This can happen because of the structure change of the sample under these heating rates.

Results of SEM-EDX, XRD and RAMAN are that FG specimen consists of carbon with negligible impurities in it. The broad peaks in XRD and RAMAN are indications of amorphous material in the sample.

From morphological and structural aspects, FG sample is in agglomerated form and consist mostly of amorphous carbons with graphite-2H in it and their chain like and pseudospherical structure is observed with TEM. Deviations of interatomic distances in the order of mesoscopic scale ($\simeq$1 nm) are observed with TEM.

In industry, equipment named soot blowers are used to remove soot from the combustion chamber of furnaces. Even though they are effective at cleaning the combustion chamber and the surface of heater tubes, they are not capable of removing soot formed in the vicinity or inside of burner tips.

In this study, experiments conducted, and techniques used are helped the author to propose a method for removing the soot from inside of the burner tips. Usually, in refineries, in order to prevent any issues because of the burner clogging is site checking the burners from observation windows of the furnaces. This is a manual process and requires relying on the operators' observation skills. From the results of this study, it can be concluded that the specimen can be eliminated by heating it up to 700 °C without the need for disassembling the burner for maintenance breaks.

5.2. Future Study

In this section, some solution methods are proposed in order to prevent or delay the unintentional soot formation. The success or performance of these solutions are not in the scope of this thesis and needs further study.

- Air barrier around nozzle: Some burner tips have a conical design. For these types of burner tips, a hollow ring with holes facing the inside of the ring and angled in a way that the leaving air stream from the holes will flow along the burner tips surface can be designed. The use of this piece is, the continuous air jet around the nozzle can help the soot being formed not to hold on to the surface of the burner tip. The effect of the additional air jet should be investigated since it can interfere with the burner tip's fuel injection performance.

- Surface topology of nozzle tip: One of the reasons of soot formation inside of the burner nozzles is the surface finishing grade. This is because if the surface is not fine enough, the fuel molecules start to stick on the walls of the burner holes. This process starts at the molecular level and once it starts it will

continue building up until the burner is disassembled for the maintenance and cleaned up. The finer the surface the harder the fuel particles stick to the surface of the nozzle. From experience, when the lower quality burner tips with rough surface finish used in the burners, the cleanup frequency increases drastically. The effect of the finishing grade can be further studied.

- Filtering the fuel: In every process in refineries, there are impurities exists in the products. Fuel used to fire burners may also have impurities such as corrosion and molecular level degradations may occur while the fuel is being transferred to the burner with pipelines. These impurities must be filtered out both for the combustion efficiency and the burner's uptime and reliability. These impurity particles may also stick to the walls of the burner nozzle and initiate the chain of particle build up until the nozzle gets clogged. The effect of filtration can be further studied.

REFERENCES

[1] "Electricity Generation Costs," 2016.

[2] J. Shen, F. Li, D. Shi, H. Li, and X. Yu, "Factors Affecting the Economics of Distributed Natural Gas-Combined Cooling, Heating and Power Systems in China: A Systematic Analysis Based on the Integrated Decision Making Trial and Evaluation Laboratory-Interpretative Structural Modeling (DEMATEL-ISM)," *Energies*, vol. 11, no. 9, p. 2318, 2018.

[3] S. Mokhatab, *Handbook of natural gas transmission and processing : principles and practices*. .

[4] S. Faramawy, T. Zaki, and -E Sakr, "Natural gas origin, composition, and processing: A review," 2016.

[5] BP, "67 th edition Contents is one of the most widely respected," *Stat. Rev. World Energy*, pp. 1–56, 2018.

[6] EPDK, "EPDK (Enerji Piyasası Düzenleme Kurumu) 2017 Yılı Elektrik Piyasası Gelişim Raporu," 2017. [Online]. Available: http://epdk.gov.tr/Detay/Icerik/3-0-0-102/yillik-rapor-elektrik-piyasasi-gelisim-raporlari. [Accessed: 06-Jan-2019].

[7] R. F. Gas, "Combustion of Refinery Fuel Gas."

[8] A. Kaupp, "The soot and scale problems," pp. 1–12.

[9] Z. A. Mansurov, "Soot formation in combustion processes (review)," *Combust. Explos. Shock Waves*, vol. 41, no. 6, pp. 727–744, 2005.

[10] "RUP - Tüpraş." [Online]. Available: https://www.tupras.com.tr/en/rup. [Accessed: 12-Feb-2018].

[11] A. Rohani, K. Sharifi, and R. Golpasha, "Calcinations of Petroleum Coke," in *3rd International Conference on Chemical, Ecology and Environmental Sciences*, 2014, no. April, pp. 100–102.

[12] OCI, "Petroleum Coke : the coal hiding in the Tar Sands," *Oil Chang. Int.*, no. January, 2013.

[13] A. Andrews *et al.*, "Petroleum Coke: Industry and Environmental Issues Specialist in Energy Policy," *Fuel*, vol. 80, no. 2, p. 25, 2013.

[14] A. Andrews and R. K. Lattanzio, "Petroleum Coke: Industry and Environmental Issues Specialist in Energy Policy," p. 25, 2013.

[15] H. Al-Haj-Ibrahim and B. I. Morsi, "Desulfurization of Petroleum Coke: A

Review," *Ind. Eng. Chem. Res.*, vol. 31, no. 8, pp. 1835–1840, Aug. 1992.

[16] S. Birghila, I. Carazeanu Popovici, and A. Dumitru, "Study on physical-chemical properties of petroleum cokes," *Rom. Reports Phys.*, vol. 56, no. 7–8, pp. 976–982, 2011.

[17] by D. John Elliott Director and C. Foster Wheeler, "Managing Shot Coke: Design & Operation."

[18] J. M. Lee, J. J. Baker, J. G. Rolle, and R. Llerena, "Characterization of green and calcined coke properties used for aluminum anode-grade carbon," *ACS Div. Fuel Chem. Prepr.*, vol. 43, no. 2, pp. 271–275, 1998.

[19] C. E. Baukal, *The john zink hamworthy combustion handbook, second edition: Volume 1 - fundamentals*, vol. 1. 2012.

[20] Spectra Sensors Inc., "Hydrogen Sulfide in Refinery Fuel Gas." [Online]. Available: https://www.spectrasensors.com/23402/. [Accessed: 12-May-2019].

[21] T. H. Fletcher, J. L. Ma, J. R. Rigby, A. L. Brown, and B. W. Webb, "Soot in coal combustion systems," *Prog. Energy Combust. Sci.*, vol. 23, no. April 1996, pp. 283–301, 1997.

[22] H. Bockhom, *Soot Formation in Combustion*. .

[23] D. C. Siegla, *Particulate Carbon*. 1982.

[24] J. Lahaye and G. Prado, "Morphology and Internal Structure of Soot and Carbon Blacks," in *Particulate Carbon*, Boston, MA: Springer US, 1981, pp. 33–55.

[25] F. A. Atiku, "Combustion of Bio-oil and Heavy Fuel Oil," no. November, pp. 1–297, 2015.

[26] E. D. Dikio, "Morphological characterization of soot from the atmospheric combustion of kerosene," *E-Journal Chem.*, vol. 8, no. 3, pp. 1068–1073, 2011.

[27] V. Petit, A. Le Rouge, F. Béclin, H. El Hamzaoui, and L. Bigot, "Experimental Study of SiO_2 Soot Deposition using the Outside Vapor Deposition Method," *Aerosol Sci. Technol.*, vol. 44, no. 5, pp. 388–394, 2010.

[28] K. H. Homann, "Carbon formation in premixed flames," *Combust. Flame*, vol. 11, no. 4, pp. 265–287, Aug. 1967.

[29] A. Marchand, "Thermal variation of the magnetic susceptibility of some carbon blacks," ... *Wkly. Render. ...*, 1954.

[30] H. G. Wagner, "Soot formation in combustion," *Symp. Combust.*, vol. 17, no. 1, pp. 3–19, Jan. 1979.

[31] P. A. Tesner and S. V. Shurupov, “Soot formation during pyrolysis of naphthalene, anthracene and pyrene,” *Combust. Sci. Technol.*, vol. 126, no. 1–6, pp. 139–151, 1997.

[32] P. Visser, V. M. Van Essen, and H. B. Levinsky, “IGRC paper 2014 Predictive method for soot formation final,” 2014.

[33] A. Thomas, “Carbon formation in flames,” *Combust. Flame*, vol. 6, pp. 46–62, Jan. 1962.

[34] J. Jarosinski, *Combustion Phenomena: Selected Mechanisms of Flame Formation, Propagation, and Extinction*. 2009.

[35] H. B. Palmer and C. F. Cullis, “Chemistry and Physics of Carbon,” 1965, p. 265.

[36] M. Cowperthwaite and S. H. Bauer, “Estimation of Molecular Parameters of C/H Fragments,” *J. Chem. Phys.*, vol. 36, no. 7, pp. 1743–1753, Apr. 1962.

[37] K. M. Leung, R. P. Lindstedt, and W. P. Jones, “A simplified reaction mechanism for soot formation in nonpremixed flames,” 1991.

[38] I. I. T. Kharagpur, N. Phase, and I. I. W. Coursesiitkgp, “Module 5 : Combustion Technology Lecture 33 : Combustion air calculation *,” pp. 1–9.

[39] I. Glassman, “Soot formation in combustion processes,” *Symp. Combust.*, vol. 22, no. 1, pp. 295–311, Jan. 1989.

[40] H. Böhm *et al.*, “The influence of pressure and temperature on soot formation in premixed flames,” *Symp. Combust.*, vol. 22, no. 1, pp. 403–411, Jan. 1989.

[41] H. Mätzing and H. G. Wagner, “Measurements about the influence of pressure on carbon formation in premixed laminar C2H4-air flames,” *Symp. Combust.*, vol. 21, no. 1, pp. 1047–1055, Jan. 1988.

[42] J. J. Macfarlane, F. H. Holderness, and F. S. E. Whitcher, “Soot formation rates in premixed C5 and C6 hydrocarbon□air flames at pressures up to 20 atmospheres,” *Combust. Flame*, vol. 8, no. 3, pp. 215–229, Sep. 1964.

[43] D. T. A. T. William Arthur Bone, *Flame and Combustion in Gases*. Longmans, Green, 1927.

[44] M. Kunugi and H. Jinno, “Determination of size and concentration of soot particles in diffusion flames by a light-scattering technique,” *Symp. Combust.*, vol. 11, no. 1, pp. 257–266, Jan. 1967.

[45] V. Arun, A. Arulkumar, B. Kavibalan, G. Nandhakumar, and G. Paramaguru, “Effectiveness Of Sootblowers In Boilers Thermal Power Station,” pp. 1–7.

[46] T. R. Barfknecht, “Toxicology of soot,” *Prog. Energy Combust. Sci.*, vol. 9, no.

3, pp. 199–237, Jan. 1983.

[47] "WHO | Household air pollution: Health impacts," *WHO*, 2018.

[48] "WHO | Chapter 4," *WHO*, 2010.

[49] B. Li and R. D. Gonzalez, "The measurement of small amounts of coke by a sensitive TGA/FTIR technique," *Catal. Letters*, vol. 54, no. 1/2, pp. 5–8, 1998.

[50] P. Keliang, X. Wenguo, and Z. Changsui, "Investigation on pyrolysis characteristic of natural coke using thermogravimetric and Fourier-transform infrared method," *J. Anal. Appl. Pyrolysis*, vol. 80, no. 1, pp. 77–84, 2007.

[51] Z. Shi *et al.*, "Purification of single-wall carbon nanotubes," *Solid State Commun.*, vol. 112, no. 1, pp. 35–37, 1999.

[52] B. G. Ma, X. G. Li, L. Xu, K. Wang, and X. G. Wang, "Investigation on catalyzed combustion of high ash coal by thermogravimetric analysis," *Thermochim. Acta*, vol. 445, no. 1, pp. 19–22, Jun. 2006.

[53] A. Toptas, Y. Yildirim, G. Duman, and J. Yanik, "Combustion behavior of different kinds of torrefied biomass and their blends with lignite," *Bioresour. Technol.*, vol. 177, pp. 328–336, Feb. 2015.

[54] N. S. Yuzbasi and N. Seluk, "Air and oxy-fuel combustion behaviour of petcoke/lignite blends," *Fuel*, vol. 92, no. 1, pp. 137–144, Feb. 2012.

[55] S. Lebedkin *et al.*, "Single-wall carbon nanotubes with diameters approaching 6 nm obtained by laser vaporization," *Carbon N. Y.*, vol. 40, no. 3, pp. 417–423, Mar. 2002.

[56] W. Jiang, G. Nadeau, K. Zaghib, and K. Kinoshita, "Thermal analysis of the oxidation of natural graphite — effect of particle size," *Thermochim. Acta*, vol. 351, no. 1–2, pp. 85–93, Jun. 2000.

[57] L. S. K. Pang, J. D. Saxby, and S. P. Chatfield, "Thermogravimetric analysis of carbon nanotubes and nanoparticles," *J. Phys. Chem.*, vol. 97, no. 27, pp. 6941–6942, 1993.

[58] A. Dychalska, P. Popielarski, W. Franków, K. Fabisiak, K. Paprocki, and M. Szybowicz, "Study of CVD diamond layers with amorphous carbon admixture by Raman scattering spectroscopy," *Mater. Sci.*, vol. 33, no. 4, pp. 799–805, Dec. 2015.

[59] M. Alfè, B. Apicella, R. Barbella, J.-N. N. Rouzaud, A. Tregrossi, and A. Ciajolo, "Structure-property relationship in nanostructures of young and mature soot in premixed flames," *Proc. Combust. Inst.*, vol. 32 I, no. 1, pp. 697–704, Jan. 2009.

[60] M. Alfè, B. Apicella, J. N. Rouzaud, A. Tregrossi, and A. Ciajolo, "The effect

of temperature on soot properties in premixed methane flames," *Combust. Flame*, vol. 157, no. 10, pp. 1959–1965, 2010.

[61] S. H. Park, M. Y. Choi, and A. Yozgatligil, "Nanostructure of soot collected from ethanol droplet flames in microgravity," *Combust. Sci. Technol.*, vol. 181, no. 9, pp. 1164–1186, 2009.

[62] L. Castoldi, R. Matarrese, L. Brambilla, A. Serafini, M. Tommasini, and L. Lietti, "Effect of potassium on a model soot combustion: Raman and HRTEM evidences," *Aerosol Sci. Technol.*, vol. 50, no. 4, pp. 405–415, Apr. 2016.

[63] A. M. Vargas and Ö. L. Gülder, "Pressure dependence of primary soot particle size determined using thermophoretic sampling in laminar methane-air diffusion flames," *Proc. Combust. Inst.*, vol. 36, no. 1, pp. 975–984, 2017.

[64] UOP, "UOP CCR Platforming^{TM} Process," 2013. [Online]. Available: https://www.uop.com/reforming-ccr-platforming/#. [Accessed: 22-Apr-2018].

[65] B. Domergue, P. Y. L. Goff, and J. Ross, "Octanizing reformer options," *Pet. Technol. Q.*, vol. 11, no. 1, pp. 67–73, 2006.

[66] N. Iwashita, "X-ray Powder Diffraction," in *Materials Science and Engineering of Carbon*, 2016, pp. 7–25.

[67] G. Okyay, "Impact of the morphology of soot aggregates on their radiative properties and the subsequent radiative heat transfer through sooty gaseous mixtures," pp. 48–49, 2016.

[68] M. Baghirzade, "Investigation of Turkish lignites and biomass at high heating rates by using wire mesh apparatus," 2018.

[69] D. Vamvuka, N. El Chatib, and S. Sfakiotakis, "Measurements of ignition point and combustion characteristics of biomass fuels and their blends with lignite," *Combustion*, no. January 2011, p. 95, 2011.

[70] L.-E. Åmand and C. J. Tullin, "The Theory Behind FTIR analysis Application Examples From Measurement at the 12 MW Circulating Fluidized Bed Boiler at Chalmers."

APPENDICES

A. Detailed Results

A1. Additional Results of FTIR

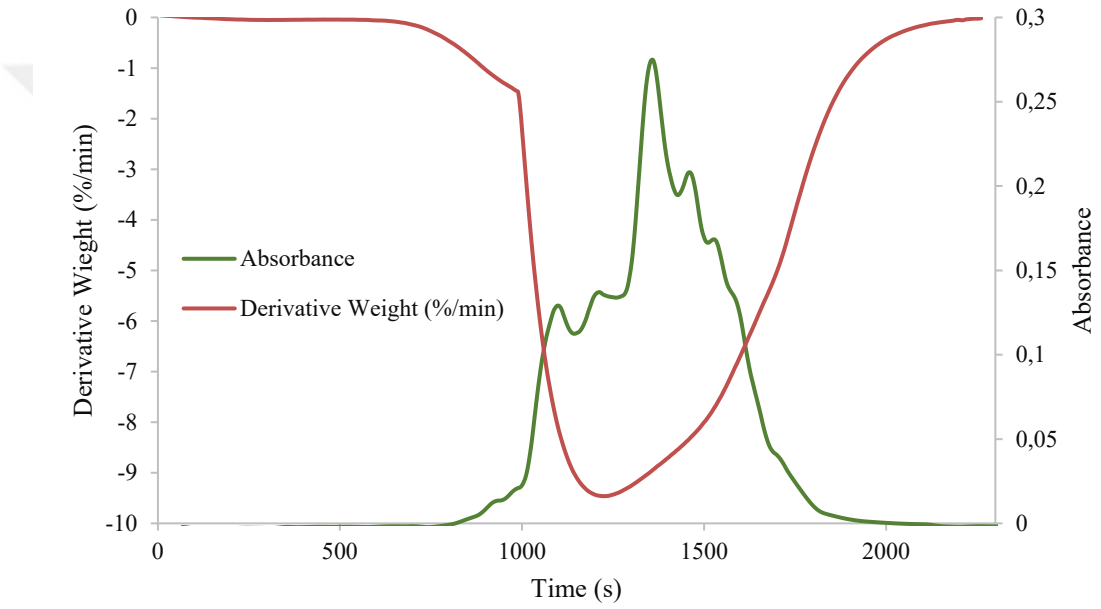

Figure A.1 DTG profile and FTIR absorbance spectrum of CO_2 of the isothermal combustion of the 75-106 µm fuel gas soot (FG) sample at 700 ºC of repetition experiment

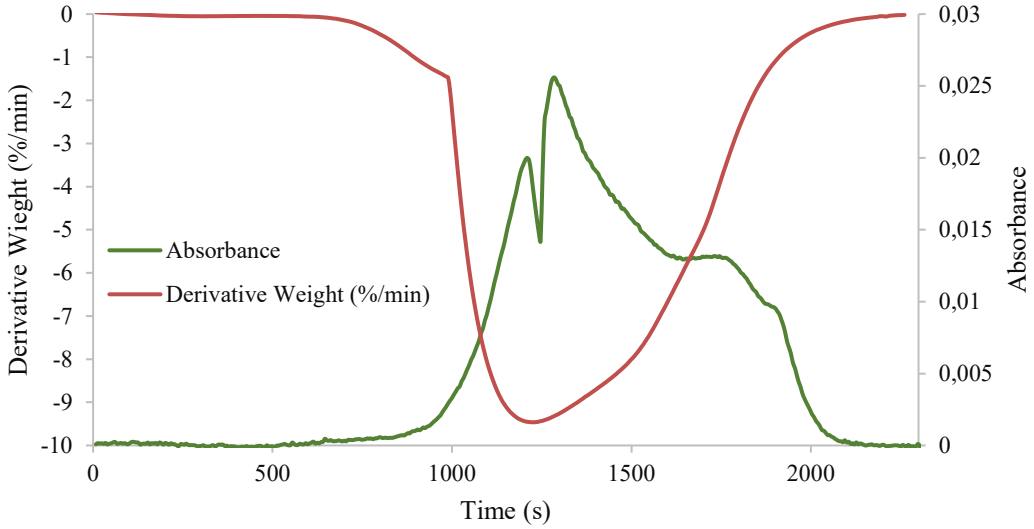

Figure A.2 DTG profile and FTIR absorbance spectrum of CO of the isothermal combustion of the 75-106 µm fuel gas soot (FG) sample at 700 ºC of repetition experiment

A.2. Extended Results of XRD

Table A.1 Qualitative analysis results of XRD

Qualitative Analysis Results			
Phase name	**Formula**	**Figure of merit**	**Phase reg. detail**
Graphite-2H	C	0.2586296318068891	411487 (ICDD)
Phase name	**Formula**	**Space group**	**Phase reg. detail**
Graphite-2H	C	194 : P63/mmc	411487 (ICDD)

Table A.2 Peak list from XRD data

Peak List						
2-theta (deg)	**d (A)**	**Height (cps)**	**Int. I (cps deg)**	**FWHM (deg)**	**Size**	**Phase name**
25.771(18)	3.454(2)	695(24)	3720(10)	3.04(3)	28.0(3)	Graphite-2H, (0,0,2)
43.23(8)	2.091(4)	80(8)	479(71)	3.71(19)	24.1(13)	Graphite-2H, (1,0,0)
46.8867(0)	193.615	0	0(40)	3.43275(0)	263.453	Graphite-2H, (1,0,2)
52.3(2)	1.746(7)	20(4)	293(38)	7.7(8)	12.0(12)	Graphite-2H, (0,0,4)
78.5(3)	1.218(3)	14(3)	82(5)	5.2(3)	20.7(12)	Graphite-2H, (1,1,0)

A.3. Detailed EDX results

Table A.3 EDX results of the sample images by scan number

Scan #	Element	Wt %	Atomic %	Error %	Net Int. %	Net Error %	K Ratio	Z	R	A	F
1	C	100.00	100.00	1.42	84.38	0.56	1.0000	1.0000	1.0000	1.0000	1.0000
2	C	49.48	59.97	10.85	26.79	2.78	0.1427	1.0360	0.9824	0.2785	1.0000
	O	35.05	31.89	12.58	19.48	3.32	0.0556	0.9904	1.0018	0.1603	1.0000
	Al	5.76	3.11	8.14	17.40	4.24	0.0361	0.8797	1.0379	0.7062	1.0097
	Si	9.71	5.03	6.37	31.33	3.01	0.0664	0.8988	1.0437	0.7577	1.0039
3	C	100.00	100.00	1.27	722.13	0.41	1.0000	1.0000	1.0000	1.0000	1.0000
4	C	100.00	100.00	1.33	600.05	0.47	1.0000	1.0000	1.0000	1.0000	1.0000

A.4. Closeup View of SEM Images

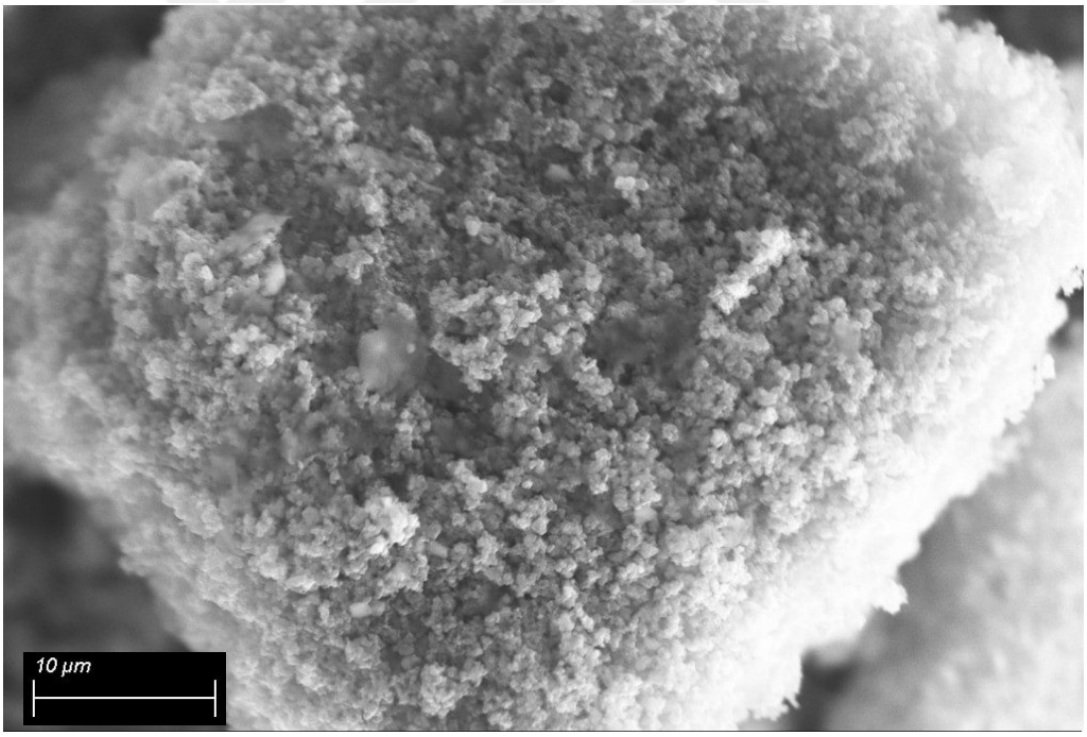

Figure A.3 SEM image of 0-75 µm particle sized fuel gas soot (FG) sample

A.5. Closeup View of TEM Micrograms

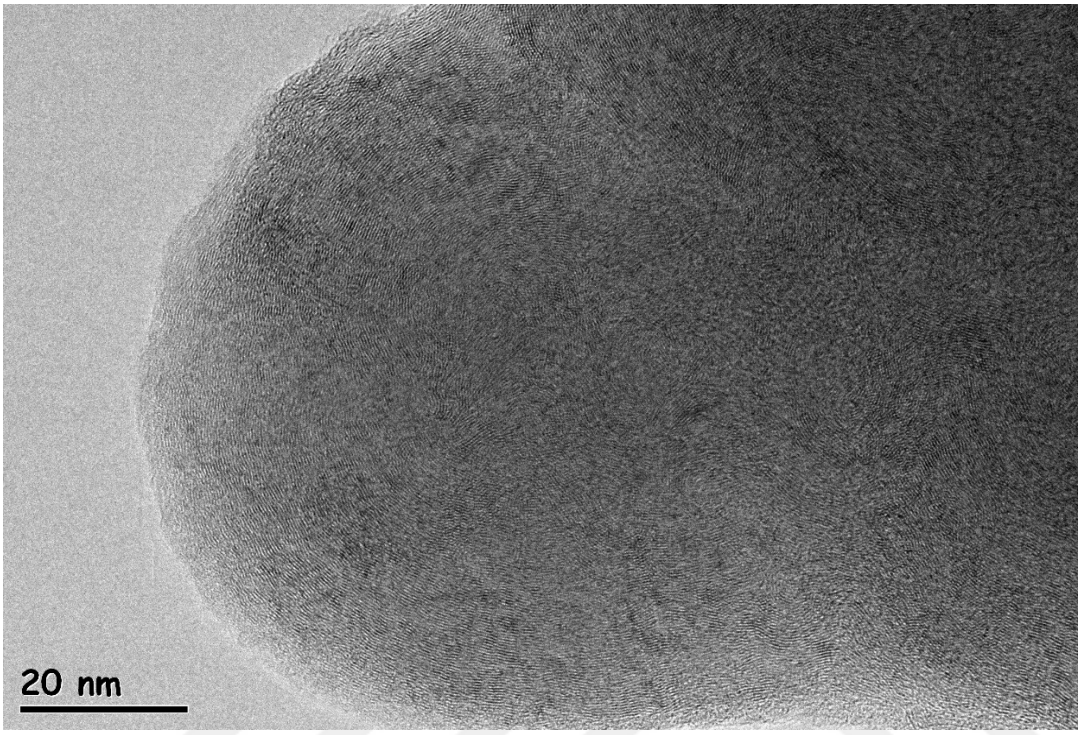

Figure A.4 HRTEM microgram of FG soot sample